Pre-beam maps of the sPHENIX electromagnetic calorimeter

sPHENIX internal note

Weihu Ma (Fudan University), Mason Housenga (UIUC),
Caroline Riedl (UIUC), Tim Rinn (BNL),
Sean Stoll (BNL), Eric Thorsland (UIUC)
for the sPHENIX EMCal group

August 17, 2022

Version 2.0

Maps of the sPHENIX EMCal in absorber-block density, light-transmission yield, relative scintillation response, and cosmic MPV are presented. All maps were collected before the arrival of RHIC beams for sPHENIX and will serve as starting point for an advanced calibration of the EMCal with neutral pions produced in collisions of gold nuclei (Au-Au) or protons (p-p). Section 1 of this note summarizes the sPHENIX EMCal properties and construction. Section 2 summarizes the block and channel properties and how they were obtained. Sector maps are presented in section 3 and the documentation of the code to generate the maps is given in section 4. Lastly, the appendix lists some production details that may be useful for the management of a future calorimeter project.

Contents

1 The sPHENIX EMCal **3**

1.1 Overview . . . 3

1.2 From blocks to sectors . . . 5

1.3 Physics requirements and beam tests . . . 8

1.4 Block, module, sector construction and testing . . . 9

1.5 From blocks to towers = readout channels . . . 13

2 Block and channel (tower) properties **15**

2.1 Block density . . . 15

2.2 Light-transmission yield and uniformity . . . 16

2.3 Scintillation response . . . 16

2.4 UIUC database . . . 16

2.5 BNL DBN maps . . . 17

2.6 Cosmic MPV . . . 21

2.7 Correlations between block properties . . . 24

3 Sector maps **28**

3.1 Maps ordered by sector serial number . . . 29

3.2 Maps ordered by sector physical location . . . 33

4 Documentation of sector-map code **41**

4.1 Input data and map generation . . . 41

4.2 Switching between channels and blocks . . . 42

List of tables **44**

List of figures **45**

Bibliography **46**

A Raw material used at UIUC **48**

B Person power at UIUC **59**

1 The sPHENIX EMCal

1.1 Overview

The sPHENIX electromagnetic calorimeter (EMCal) is a sampling SPACAL (spaghetti calorimeter) made of 6,144 absorber blocks with each 2,688 scintillating fibers embedded in a matrix of tungsten powder and epoxy, see Fig. 1.1 for an overview sketch.

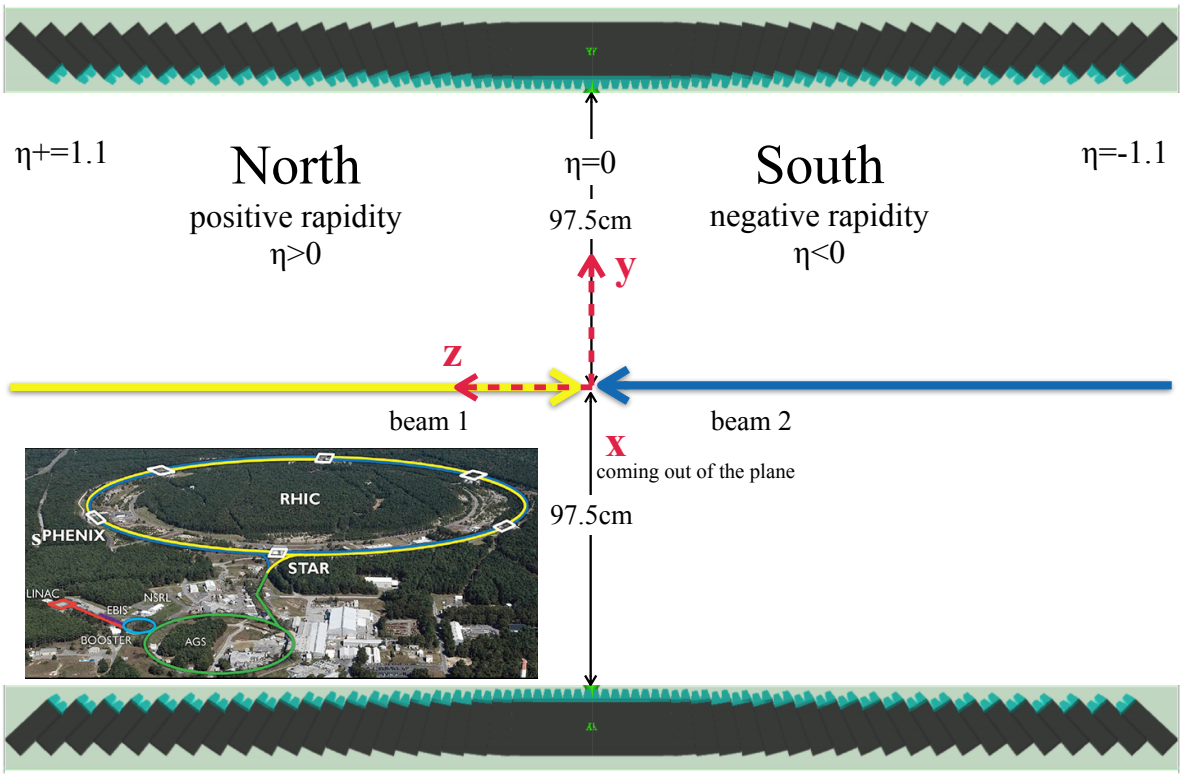

Figure 1.1: sPHENIX EMCal slice in the yz-plane at $x = 0$ and indication of the convention for beams and sign of rapidity. The sPHENIX experiment is located at RHIC's IP8, where the "yellow" beam goes South and the "blue" beam North. The coordinate system is right-handed with the x-direction pointing out of the RHIC ring (= West), y pointing upwards, and z pointing North, which is also the direction of the SC magnetic field.

The fibers are held in position with brass meshes spaced along the length of the block. They have a diameter of 47 mm and are spaced 1 mm apart from each other.

Each block has four towers or readout channels with four SiPMs each, resulting in a total of 24,576 readout channels, 98,304 SiPMs, and 16.5 million fibers. The EMCal covers a pseudo-rapidity range of about $|\eta| < 1.1$ and full azimuth ϕ. The single-tower angular resolution is (polar $\times$ azimuthal) = $(\Delta\eta \times \Delta\phi) = 0.024 \times 0.024$, which means that the precise rapidity coverage of the EMCal is $|\eta| \leq 1.152$. The often-quoted $|\eta| < 1.1$ is the rapidity coverage of the outer hadronic calorimeter (oHCal).

The absorber blocks have an average density of 9.2 g/cm^3. The average tower has 20 radiation lengths (X_0) for electromagnetically interacting particles, with $X_0 = 7$ mm. One EMCal tower has the size of

about $(1.1\ R_{\mathrm{M}})^2$, with the Moliere radius[1] $R_{\mathrm{M}} = 2.3$ cm. The EMCal also measures about one interaction length of hadronic showers. The EMCal sampling fraction is about 2.1% in average.

The inner hadronic calorimeter (iHCal) immediately following the EMCal is used to catch the tails of pion showers in order to veto hadrons. Both EMCal and iHCal are inside the sPHENIX superconducting solenoidal magnet (former BaBar magnet). The oHCal is immediately outside the magnet and measures the energy deposit of hadrons.

A sketch of the sPHENIX detector and the sequence of the calorimetric system are shown in Fig. 1.2.

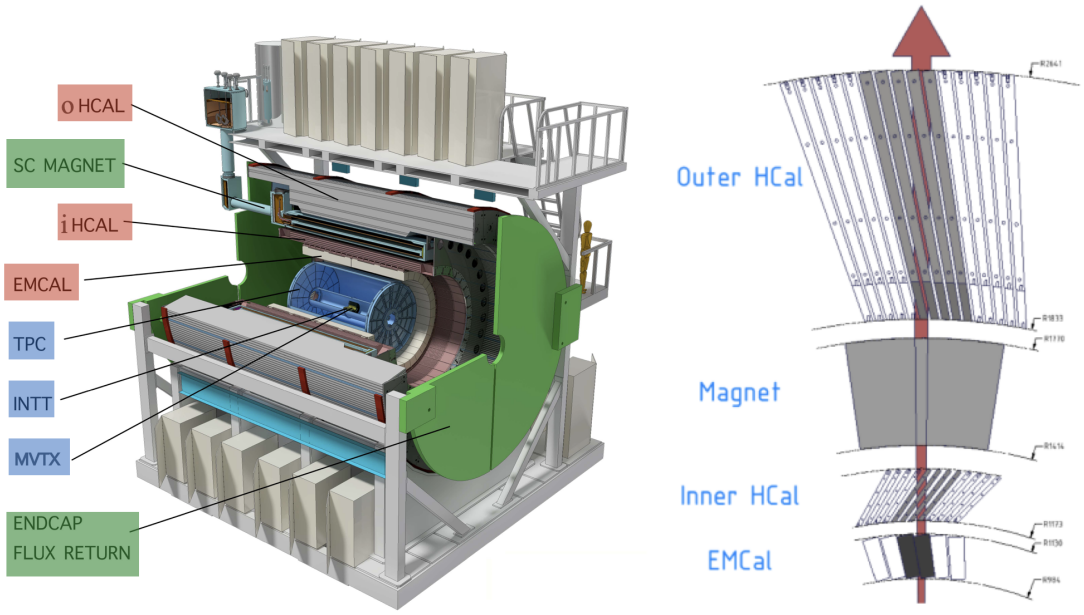

Figure 1.2: Left: sPHENIX detector (from inside to outside): the tracking system MVTX, INTT, and TPC with TPOT, the superconducting magnet, and the calorimeters EMCal, iHCal, and oHCal. Right: transverse slice through the sPHENIX calorimetric system, indicating the possible path and signal deposition of a particle.

The following references provide more details:

1. sPHENIX Technical Design Report (TDR) from 2019 [1], chapters 3 (detector) and 5 (readout), and for some early simulations also an older version of that TDR [2] (section 4.3),
2. first calorimeter test-beam paper from 2017 [3] (not yet 2D-projective),
3. second (EMCal only) test-beam paper from 2020 [4],
4. sPHENIX Beam Use Proposal (BUP) from 2022 [5] for an overview of the physics case and the EMCal requirements,

where 3. and 4. are the most recent and up-to-date documents. The EMCal was discussed in detail at the 2022 sPHENIX summer school [6].

[1] The Moliere radius is by definition the radius of a cylinder containing on average 90% of the electromagnetic shower's energy deposition. The relation between radiation length and Moliere radius is: $R_{\mathrm{M}} = 0.0265 X_0 (Z + 1.2)$, with Z the nuclear charge number. Source: wikipedia

1.2 From blocks to sectors

The EMCal blocks are tapered with a wide end and a narrow end, see Fig. 1.3.

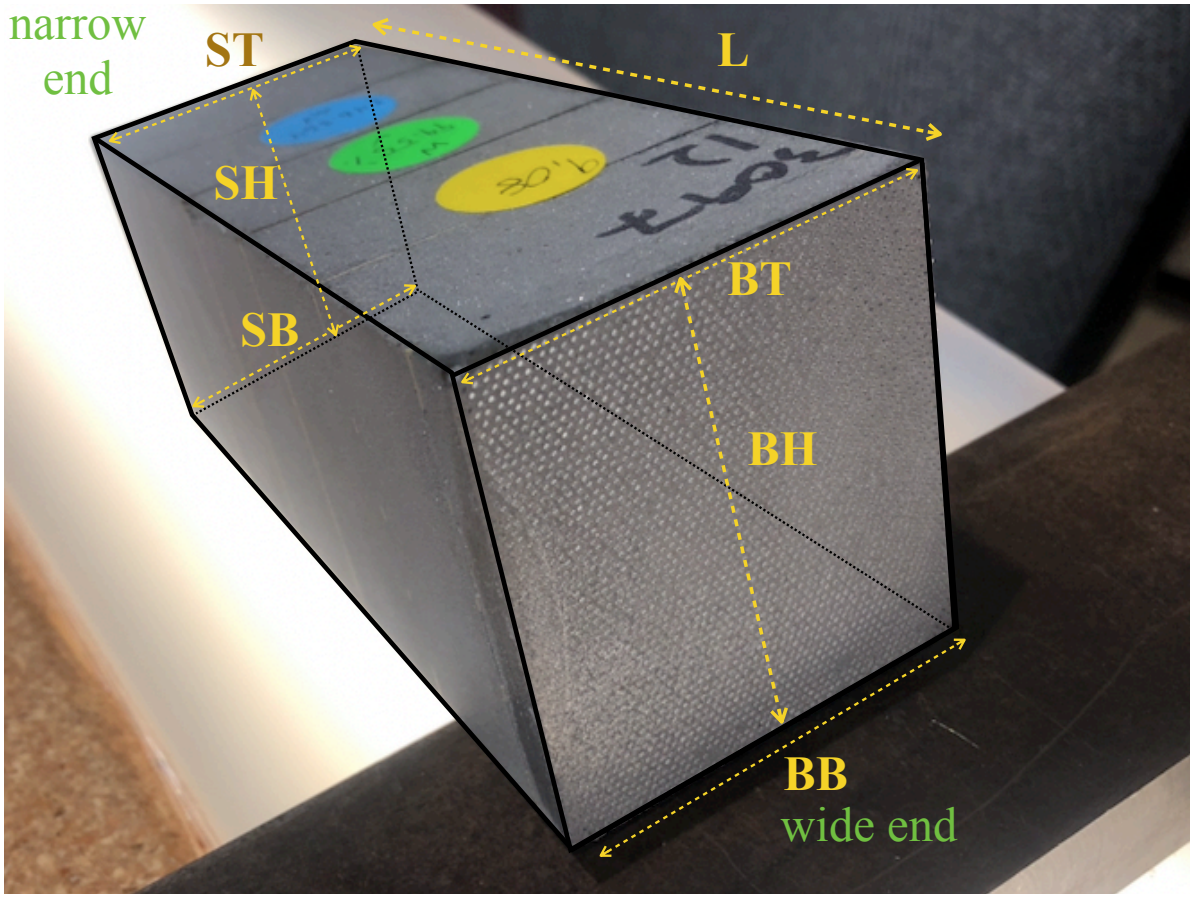

Figure 1.3: A UIUC EMCal block after machining. The average EMCal block is about length × width × height = 5 inch × 2 inch × 2 inch (16 cm × 5 cm × 5 cm) in dimensions with a volume of about 350 ml and a mass of about 3.2 kg. The block is tapered, resulting in a wide end (facing the reader, with illuminated fiber ends visible) and a narrow end. There are seven dimensional measurements defining the volume of the block, each abbreviated with two letters, where the first letter stands for Big (wide end) or Small (narrow end) and the second one for Top, Bottom, or Height. Block dimensions BB, BT, SB, and ST are mold-driven since they are defined by the dimensions of the assembled mold. The block length is denoted as L. The block has only two surfaces that are parallel to each other, the ends (except for block design 123, which has more). Written on the block with sharpie are the DBN (unique traveler) and the block type (BL). The stickers in different colors indicate the completion and results of the tests carried out.

The blocks are arranged in 64 sectors (32 North, 32 South) of 96 blocks each, creating essentially a hollow cylinder of tungsten. North sectors cover positive pseudo-rapidity ($\eta > 0$) and South sectors negative pseudo-rapidity[2] ($\eta < 0$), see Fig. 1.1.

[2] $\eta = -\ln \tan(\theta/2)$, with polar angle θ. The quantity η will be referred to as rapidity in the following.

The blocks are arranged in such a way that all of them point (almost) to the interaction point, in other words, they are **2D-projective** in both polar angle (rapidity η) and azimuthal angle (ϕ). The advantage of this 2D-projectivity will be discussed in Sec. 1.3. Consequently, the blocks start to be tilted when going from low- to high-rapidity, as shown in Fig. 1.4. While the blocks are tilted in η at 9.4° (except for block designs 123 at mid-rapidity, which are 1D-projective), the sectors are tilted in ϕ at 9.1°.

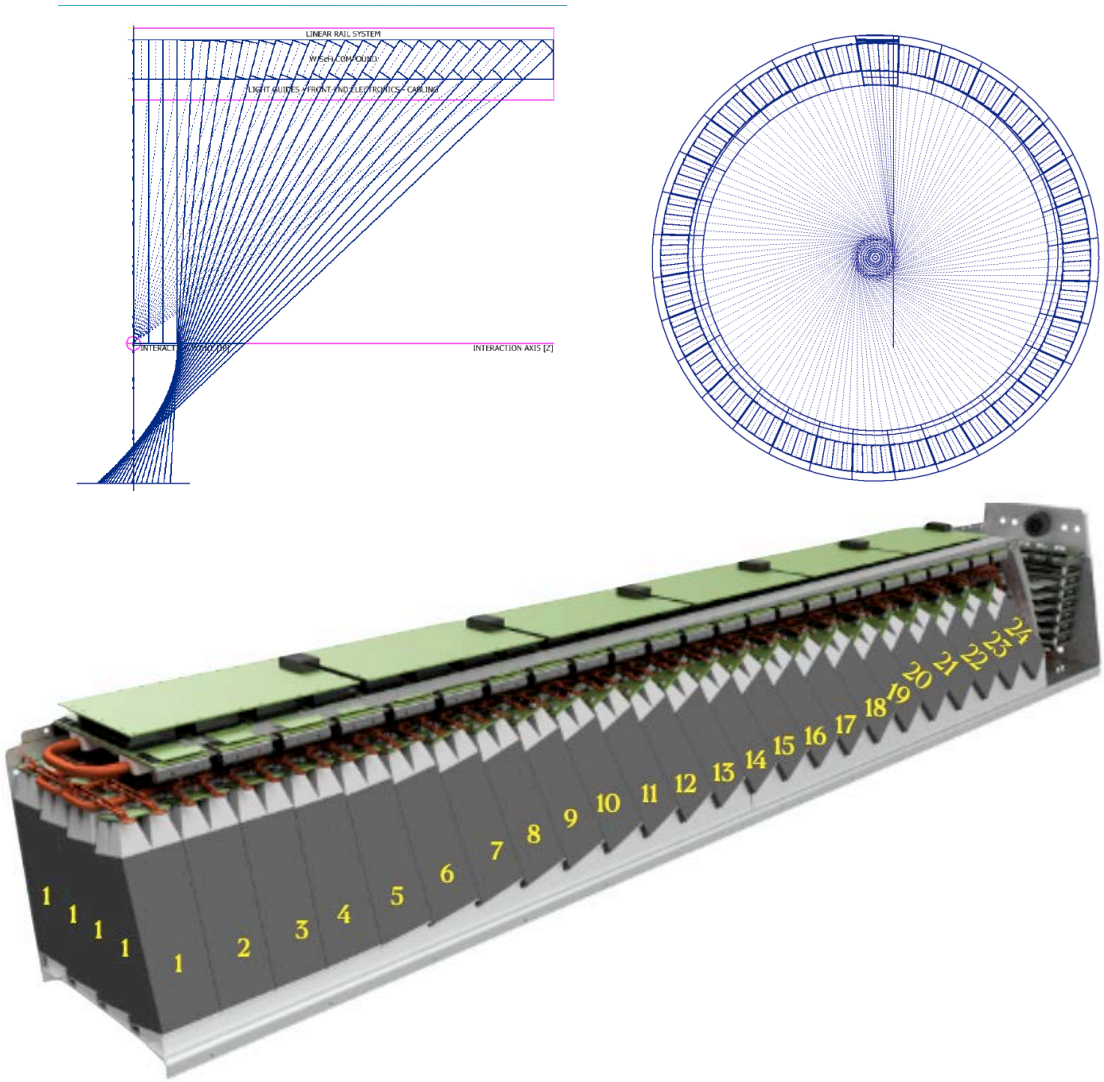

Figure 1.4: Top: demonstration of EMCal 2D-projectivity: in η (left) and in ϕ (right). To avoid effects of channeling and prevent energy leakage, the blocks are slightly offset to avoid direct pointing at the interaction point. Bottom: EMCal sector with saw teeth assembly structure, readout, and water cooling lines. The yellow numbers indicate the block type (BL).

Since the tilted blocks have to be longer and and also slightly grow or shrink in other dimensions, there are 22 different block designs referred to as **BL** 123 (identical blocks 1, 2, 3 at mid-rapidity), BL 4, ... through BL 24 (blocks at high-rapidity). The breakdown of the EMCal into sectors, blocks and towers is shown in Fig. 1.5.

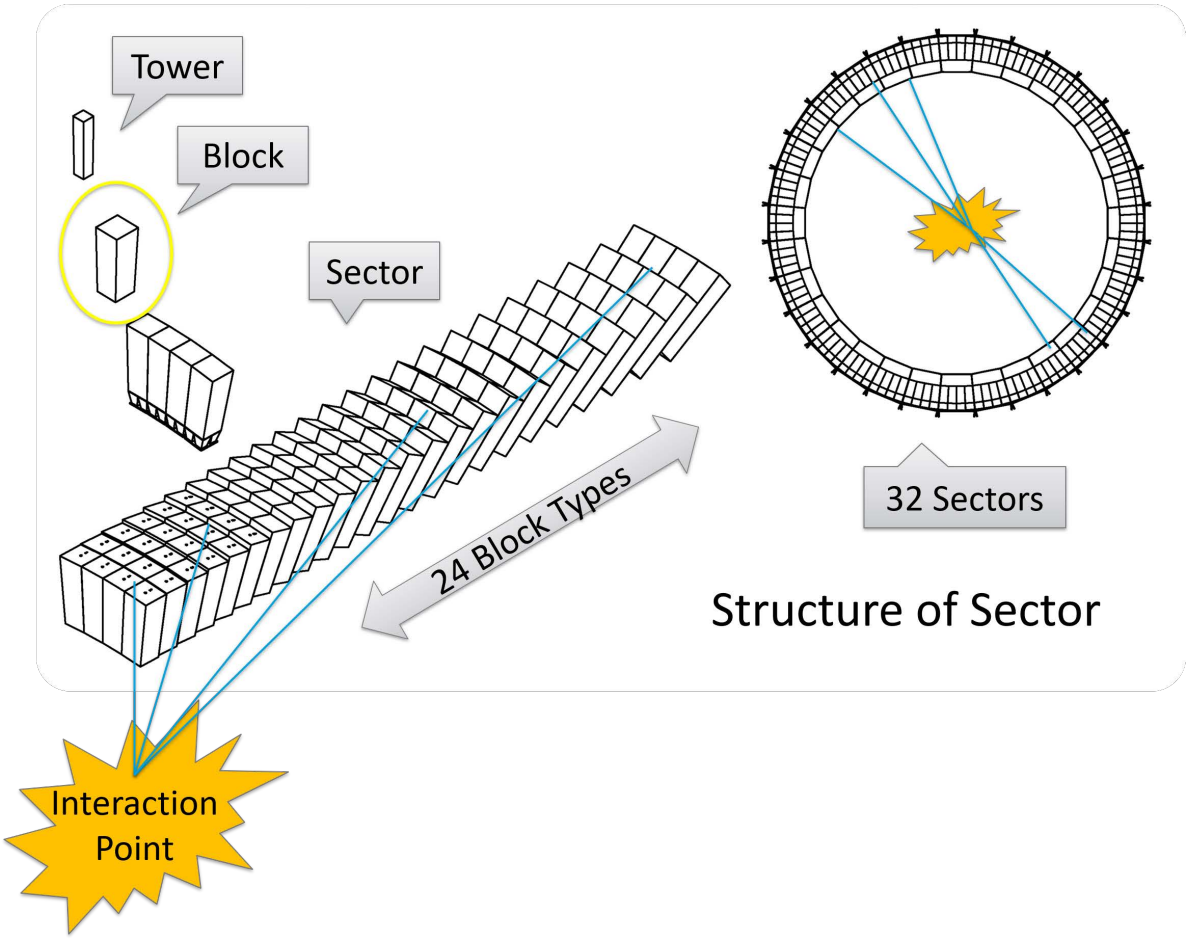

Figure 1.5: From top left to right: EMCal tower (readout channel), block, array of 4 modules (with lightguides and SiPMs), sector (note that the saw teeth assembly structure would be on top), and view along the direction of one of the beams, showing the 32 North or South sectors arranged in a tunnel-like shape.

1.3 Physics requirements and beam tests

The solid-angle coverage of the EMCal has minimal inactive areas and thus enables precise jet reconstruction over the entire central-rapidity region. The quality of the jet reconstruction efficiency and resolution is driven by the uniformity of the light-guide energy response, the degree of energy linearity, and the energy resolution [1], all of which are excellent (see test beam results below in this section). Furthermore, the EMCal will contribute to photon and Upsilon (Υ) measurements, with the Υ being a short-lived ($\sim 10^{-20}$s) b-quark b-anti-quark meson ($b\bar{b}$).

The EMCal block density and uniformity and the segmentation of the readout were chosen such that the resulting EMCal energy resolution is equal or better than $16\%/\sqrt{E} \oplus 5\%$ [4], a requirement originating from the challenges for Upsilon spectroscopy in the decay channel $\Upsilon \to ee$. The EMCal is required to discriminate between the decay electrons against the hadronic background. The electrons are expected to produce electromagnetic showers with energies of $\sim$ 4 to 10 GeV, while the underlying event background is in equivalent conditions (central Au-Au collisions) simulated to be about 320 MeV [4]. For 4 GeV electrons, the EMCal nominally rejects pions at 100:1 (90:1) with 95% (70%) efficiency for p-p (Au-Au) collisions, thus providing excellent electron-pion separation and electron ID [2].

The relative size of the underlying event determines the size of one calorimeter tower: the larger the underlying event, the smaller the tower (and thus Moliere radius) has to be in order to minimize the relative background contribution. This requirement also fixes the minimum inner radius of the EMCal. In the 2D-projective design, the blocks (almost) point to the interaction point, thus containing the electromagnetic shower in a smaller amount of blocks (towers) as they would in a 1D-projective design, see Fig. 1.4. Imagine the blocks at high rapidity would not be tilted - a trajectory from the interaction point through the blocks would cross a larger number of blocks than in the "tilted" design. This results in larger signal per tower and thus allows to better discriminate the signal against the underlying event and fluctuations. The projectivity in two dimensions significantly reduces the transverse size (in η) of the showers at large rapidity, thereby improving energy resolution and electron/hadron separation.

The energy resolution $\Delta E/E$ (often also denoted σ_E/E) of a calorimeter is typically expressed as

$$\frac{\Delta E}{E} = \frac{a}{\sqrt{E}} \oplus \frac{b}{E} \oplus c, \tag{1.1}$$

where the symbol "$\oplus$" indicates a quadratic sum. The stochastic term $a/\sqrt{E}$ arises from intrinsic statistical shower fluctuations, the noise term b/E from electronic noise of the readout chain or similar effects, and the constant term c from instrumental effects such as geometry or imperfections in detector, temperature gradient, radiation damage, etc. [7].

The sPHENIX EMCal energy resolution and linearity were measured in two test-beam campaigns at Fermilab for prototypes of the 1D-projective design [3] and the 2D-projective design [4] [8] [9]. Here, only the latter will be reported since the used 2D-projective "v2.1 prototype" design was realized at the end of the day in the construction of the sPHENIX EMCal. The energy resolution was measured using Fermilab electron beams of energies between 2 GeV and 28 GeV and separately applying two different correction methods of position dependence:

1. the **hodoscope-position dependent** correction used a scintillation hodoscope to measure the beam position and yielded

$$\frac{\Delta E}{E} = 3.5\%\ (\pm 0.1\%) \oplus \frac{13.3\%\ (\pm 0.2\%)}{\sqrt{E}}, \tag{1.2}$$

2. the **cluster-position-dependent** correction used the measured shower position in the EMCal itself and yielded

$$\frac{\Delta E}{E} = 3.0\% \ (\pm 0.1\%) \oplus \frac{15.4\% \ (\pm 0.3\%)}{\sqrt{E}}. \tag{1.3}$$

Both Eq. 1.2 and Eq. 1.3 satisfy the requirement to the energy resolution quoted at the beginning of this section 1.3. Deviations from linearity in the energy response were measured to be around 1‰ and are in agreement with the simulation.

1.4 Block, module, sector construction and testing

After completion of various prototyping campaigns at UIUC 2015-2019, the EMCal **absorber blocks** were constructed from the raw material at three sites from 2019 through 2021: University of Illinois at Urbana-Champaign - UIUC (USA), Fudan University in Shanghai (China), the China Institute of Atomic Energy - CIAE in Beijing (China) and Peking University - PKU (China), see Tab. 1.1. The blocks for the so-called **pre-production sectors S1-12** were entirely built at UIUC, while the blocks for the **production sectors S13-64** were built at UIUC and in China.

Starting with Sector 13, the Chinese institutions took over the construction of the high-rapidity blocks (BL 19-24) after the DoE had de-scoped the project. Representatives from Fudan University visited UIUC in summer 2018 to become familiar with the block production. While this document details the production steps at UIUC with all steps performed in-house at the Nuclear Physics Lab (NPL), the procedures at Fudan and CIAE / PKU are very similar [10]. The Chinese blocks were machined by outside companies and some of the used materials differ as detailed in Tab. 1.1. The **material suppliers and specifications** were as follows (were applicable, the abbreviations used during block production are indicated in square brackets):

1. Tech-Etch, http://www.techetch.com for custom-ordered photo-etched brass meshes holding the fibers in place [11]
2. [*SG*] Saint-Gobain Ceramics & Plastics, Inc., https://www.saint-gobain.com/en, BCF12 SC round, scintillating fibers dia 0.47 mm, delivered in boxes with 60-85 packets each containing 200 canes of 1.2 m length
3. [*K*] Kuraray Co., Ltd., https://www.kuraray.com, SCSF-78 scintillating fibers dia 0.47 mm
4. [HCS] H.C. Starck Tungsten LLC, https://www.hcstarck.com/en, Tungsten Metal Powder WMP GG -230 mesh, particle size $\geq 63\mu$m (but 5%), purity $\geq 99.9\%$, tap density 10.4 g/cm^3 - 10.8 g/cm^3, delivered as 60 l drums
5. [HS] Hai Sheng, http://www.grand-tungsten.com, tungsten powder, particle size 60-120μm, purity $\geq 99.95\%$, tap density 11.5 g/cm^3
6. [TJZX] Tian Jin Zhu Xin, tungsten powder (very small Chinese company)
7. Epoxy Technologies, https://www.epotek.com, EPO-TEK 301, for the casting the tungsten-fiber matrix

The UIUC material batches are listed in Appendix A. The total raw material used at UIUC (80% of produced blocks) amounts to 19 metric tons of tungsten powder, 2,000 km of scintillating fibers, 30,000 brass screens, and 650 kg of epoxy, for blocks that were actually glued into sectors (note that 10-15% of the quoted tungsten-powder weight was removed in the machining process and is not part of the EMCal).

Table 1.1: Construction sites of the EMCal absorber blocks for various block types (BL) and used materials from suppliers as listed on page 9. The total number of blocks in the completed EMCal is 6,144, of which around 80% were produced at UIUC, 15% at Fudan, and 5% at CIAE / PKU. For the majority of the blocks, SG fibers were used (SG: 91%, K: 9%). The distribution of tungsten powder is HCS ∼80%, HS ∼20%, and TJZX < 1%.

	UIUC	Fudan	CIAE / PKU
BL	all S1-12, S13-64 BL 123-18	S13-64 BL 19-24	S13-64 BL 19, 23-24
meshes	1.	1.	1.
fibers	2.	2./3.	2.
W powder	4.	5./6.	5.
epoxy	7.	7.	7.

At UIUC, block production followed a Quality Assurance Plan (QAP) agreed with BNL [12] and repeating thousands of times the precisely defined Standard Operating Procedures (SOPs) [13]. Details are given in the cited documents. Before using the raw material, it was subject to QA and preparation. All drums of tungsten powder were numbered and then tested for tap density. A small sample from about 10% of the tungsten-powder drums was investigated in a scanning electron microscope (SEM) on UIUC campus to determine the particle sizes, distributions, and chemical composition. Each box the fibers were delivered in was labeled ("fiber batch number") and one plastic sleeve of each box was opened to check that the fibers had the proper diameter (by sticking a few of them through the holes in an assembly screen) and appeared blueish in natural light. These parameters together with all delivery dates were logged in a google sheet database (see Sec. 2.4) denoted as the **UIUC database** hereafter.

In short, **absorber block production** proceeded as follows, where each block was assigned a variable status number 0-8 while it was being produced:

0. [$\omega = 0$] **Fiber-set assembly** was carried out manually with the aid of re-usable 3D-printed holders and transparent plastic cups. The fibers are held in place by six brass meshes (screens) per block, each of which contains 2668 holes in a hexagonal pattern transverse to the radial direction. The hole spacing between consecutive screens increases going from the narrow end of the block to its wide end, defining the approximate projectivity of the proto-block. Some workers found it useful to have a light source underneath the assembly cup.

1. [$\omega = 0.1$] **Fiber-set loading** in a reusable, block-type specific mold structure that consists of six delrin parts and is held together by screws. During block production in China it was found advantageous to add a reinforcing plate and clamping plates on the side of the mold to prevent the delrin from bending and keep the sides in the correct position [14]. Prior to proceeding with tungsten-powder filling, paper shims were introduced at UIUC in a few places to push edge fibers away from the inside edge of the molding form in order to prevent the fibers from being too exposed in the subsequent machining steps.

2. [$\omega = 0.2$] **Tungsten-powder filling** into the mold while resting on the vibration table to densify the powder, using a BL-type-dependent documented minimum of tungsten-powder weight.

3. [$\omega = 0.4$] **Epoxy potting / casting**, where the epoxy was added to the top of the molding form and pulled out by a vacuum pump connected to ports at the bottom of the mold. The final production mixture for one block was 110 g resin (part A), 25 g hardener (part B), and 40 g ethanol. The success of block casting depends greatly on the flow properties of the epoxy mix in combination with the granularity and mix of small/large particles of the tungsten powder. It was not necessary to add ethanol to the Chinese potting mixtures likely due to the different particle-size composition of the used tungsten powder. It was important to seal the molding form very well, for which 3M DP105 epoxy and Flex Seal aerosol spray were used at UIUC. It was found useful to warm the epoxy

Table 1.2: EMCal block grading at UIUC. A-grade, B-grade, or C-grade blocks were shipped to BNL, while blocks failing the C-grade thresholds in at least one testing category (table rows) were not shipped. The dimensions B⋆, S⋆, and L are defined in Fig. 1.3, the Δ indicating the deviations from the nominal design [11] in units of inch. "LT" denotes the percentage of light transmission per block and "LT tower" that per tower. The row or column refers to connected patterns of fibers when the block is held against a light source and visually inspected.

criteria	A-grade	B-grade	C-grade	fail
ΔB⋆ [″], ΔS⋆ [″]	±0.02	$^{+0.02}_{-0.04}$	as B-grade	if
ΔL [″]	±0.03	$^{+0.05}_{-0.1}$	as B-grade	any
density [g/cm^3]	> 8.8	> 8.7	> 8.4	C-grade
LT	≥98%	≥97%	≥96%	criterion
LT tower	≥96%	≥94%	≥92%	is
missing full row and/or double column	none	none	none	**not**
scintillation ratio	≥0.7	≥0.7	≥0.7	met

bottles on a warming table at 30°C before composing and pouring the mixture. Before proceeding, the block was left untouched on a warming table at about 30°C for 24 hours to let the epoxy cure.

4. [$\omega = 0.45$] **Block machining** proceeded in the order sides and bottom (sanding), top (shell mill), and ends to expose fibers (shell mill and as last step diamond cutting tool for polishing of the fiber ends). Prior to machining at UIUC, the block was cooled to -15°C to prevent the appearance of dark fibers in the edge rows and columns of the block. Prior to end machining at UIUC, the block was warmed up to room temperature to prevent the block ends chipping off and fibers being frayed at the block end. Since no dark-fiber edge effects were observed in China, the Chinese blocks were not cooled before machining. The diamonds used for the final end machining were replaced or regenerated on a regular basis. The mechanical precision of the EMCal absorber blocks [11] had to meet the requirement that they fit into the saw tooth assembly structure shown in Fig. 1.4 (bottom) with minimal (< 0.5 mm) gaps.

5. [$\omega = 0.75$] **Block testing** of each completed block included the measurement of dimensional compliance and density (Sec. 2.1), the light-transmission yield and uniformity (Sec. 2.2), and the scintillation response (Sec. 2.3), following strict testing protocols [15] and using documented testing software [16]. A photo of a completed UIUC block is shown in Fig. 1.3 together with the convention of dimensional measurements. More details about these tests can be found in Sec. 2.

6. [$\omega = 0.95$] **Block grading and packing** included the grading of the block as either A-, B-, C-grade, or failing (see Tab. 1.2), and the packing of non-failing blocks into rolling heavy-duty storage crates, which were custom-equipped with foam dividers to ensure a tight fit of the blocks, minimizing the possibility of movement inside the box during shipping.

7. [$\omega = 1.0$] **Block shipping** from UIUC to BNL via FedEx Air.

8. [$\omega = 0$] **Failed blocks** that do not meet at least all "C-grade" requirements in Tab. 1.2.

For each step of production and testing at UIUC, various pieces of information were logged in the UIUC database. Starting with the fiber set, each block received a unique static traveler number called **Data Base Number (DBN)**. Moreover, each block was assigned a variable weight ω with $0 \leq \omega \leq 1$ depending on its readiness (status) as defined in the enumeration. For example, when a block was finished potting, it was in status 3 and contributed a weight of 0.4 to the total number of blocks produced by UIUC. This eased the project management: to determine and log the status of the project, the weights of blocks in different stages of readiness were summed up. In the main phase of the project (October 2020 - December

2021), UIUC shipped in average 60 blocks to BNL every week (see Fig. 1.6). Details about the person power at UIUC can be found in Appendix B, with in total around 90 persons on the EMCal block project.

At UIUC, no statistically relevant effects of degradation over time in fiber count or scintillation response were found when testing the same batch of blocks over the course of several months [17]. The UIUC block production [18] and testing [19] procedures were presented in posters and UIUC Physics published a photo story about the project in fall 2021 [20]. The final project report to the collaboration was given during the January 2022 sPHENIX collaboration meeting [21].

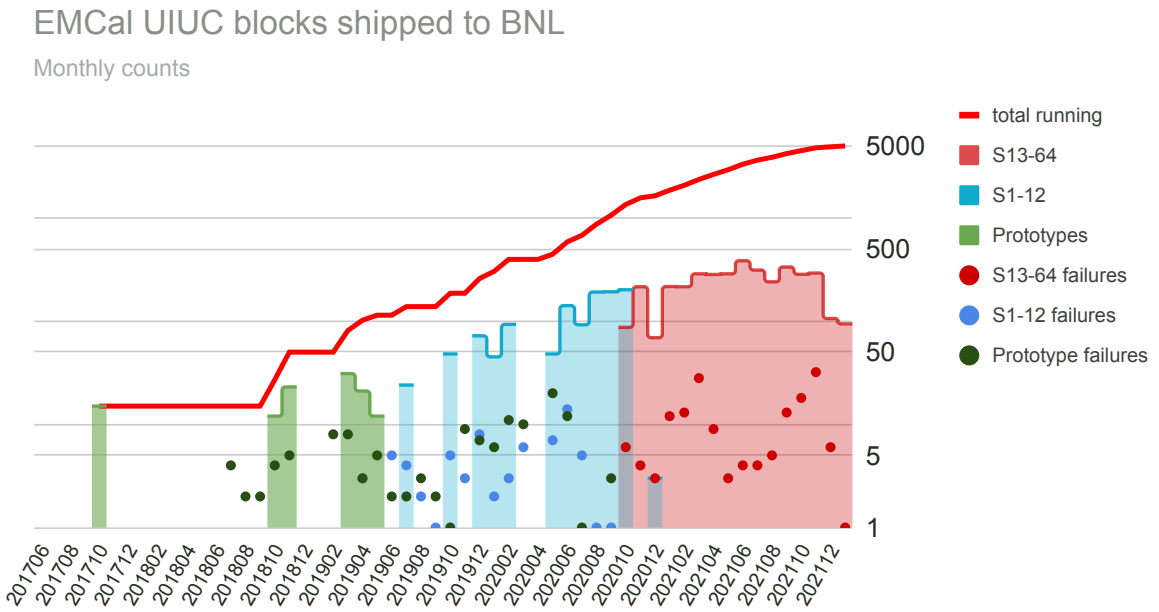

Figure 1.6: UIUC EMCal block shipments and failures 2017 - 2022.

At BNL, mirrored aluminum reflector plates were attached to the wide end of each block and molded acrylic light guides were attached to the narrow end with optical epoxy. Silicon photomultipliers (Hamamatsu S12572-015P SiPMs), mounted on a passive pcb, were optically coupled to the lightguides using silicone RTV. The resulting unit is referred to as **module**, as shown in Fig. 1.7. For the **sector assembly**, the modules were then arranged on the machined aluminum saw teeth assembly shown in Fig. 1.4 (bottom) ordered by block number (BL) and epoxied together with 3M DP460 structural epoxy. Each sector was assigned a **serial number 1...64** in the order of historical production.

Once the epoxy had cured, copper SiPM cooling loops were installed and then insulated with foam insulation tape. The preamp cooling loop assembly was then added. The preamp pcbs were then installed, cabled, and tested sequentially. Next, signal cables that carry the preamp output signals to the sector bulkhead connectors were installed, followed by the 6 interface pcbs. Finally, the interface cooling loop and control and power cable harnesses were installed and dressed, and then the sector cover was closed. Then connectors, cables, SiPM water-cooling loops, and steel housing (30 thousandths of an inch (mils) thick on the side and 60 mils on the faces) were attached. Each sector was tested during assembly and upon completion using a manual test stand with oscilloscope, for shorts, continuity, functional cable connections, electronics current draw, basic SiPM functionality (LED response, dark current), and pre-amp functionality and shaping. After assembly, groups of 8 sectors at a time went into **burn-in** testing and monitoring for at least 2 weeks, during which time the SiPM dark currents, the electronics voltages and

currents, and the temperature readouts were monitored while the sectors were powered and cooled. In the final stage of testing, the sectors were individually loaded into the cosmic ray test stand, and rotated +/- 720° to verify their mechanical robustness. The cooling loops were tested with air pressure for possible leaks. Each sector was biased at its nominal (Hamamatsu factory) Vops and recorded about 72 hours of **cosmic ray data** at 90° rotation (Sec. 2.6) verifying that all 384 detector channels were functional.

1.5 From blocks to towers = readout channels

One EMCal absorber block is segmented by the lightguides into 2×2 towers. Each tower represents 1 ADC ("physics") readout channel and is equipped with a light guide coupled to 4 SiPMs that collect the light from the fibers, as shown in Fig. 1.7. In other words, the analog signal recorded by 4 SiPMs is electronically summed into 1 analog preamp channel and then converted to a digital signal, off-detector, by the ADC. There are $96 \times 4 = 384$ distinctive ADC channels in each sector, also shown in the figure. There is no physical boundary between neighboring readout towers within a block, the boundary is determined by the lightguide positions. Adjacent towers in neighboring blocks share block edges and an epoxy bond between them. Inside the sector, channels are organized into groups of 64, each group (6 total) controlled by an interface board (IB). Interface boards are used to manage serial temperature data, bias voltages, etc. The analog signal cables from the preamps connect directly to the bulkhead connectors on the end of the sector box and do not pass through the interface boards. Each group of 64 channels (controlled by one IB) is each read out with its own digitizer.

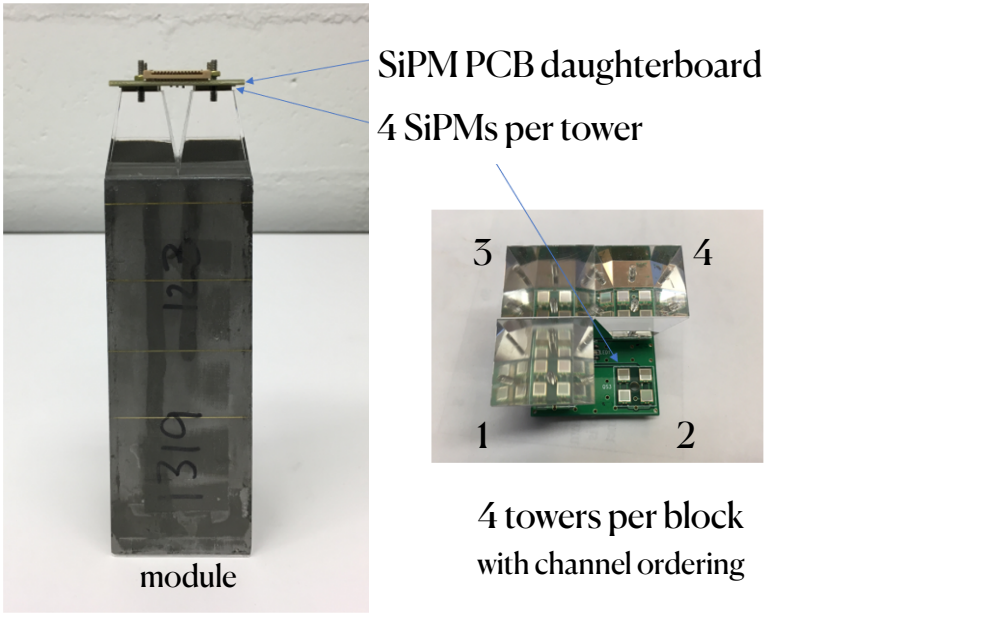

Figure 1.7: Top: EMCal module consisting of 1 block, 4 light guides, and 4x4 SiPMs. 1/4 block = 1 tower = 4 SiPMs = 1 ADC (readout) channel. Bottom: ADC channel map of 1 EMCal sector (viewed from the outer radius looking in) consisting of 96 blocks, 6 interface boards labeled IB0... IB5 with 64 ADC channels each, and 384 ADC channels, the number scheme of which is indicated in the figure.

2 Block and channel (tower) properties

A description of each property displayed in the maps in Chap. 3 is given. The tests described in Secs. 2.1-2.3 were carried out at UIUC and the Chinese sites with finished blocks. The respective criteria for "pass" or "fail" are summarized in Tab. 1.2. The bookkeeping methods are described in Secs 2.4 and 2.5 and the cosmic-ray tests at BNL in Sec. 2.6. Correlations between block density, light-transmission yield, scintillation response, and MPV are provided in Sec. 2.7.

2.1 Block density

Each block was weighed using a digital scale to determine its mass. The 7 dimensional parameters as defined in Fig. 1.3 were measured using a digital caliper. From this sets of measurements, the volume and density of the block were determined [15]. The average block density is $\rho_{\text{block}} = 9.2$ g/cm^3 (9.1 g/cm^3 for UIUC blocks, 9.7 g/cm^3 for Fudan blocks, and 9.5 g/cm^3 for CIAE blocks), and their distributions are shown in Fig. 2.1.

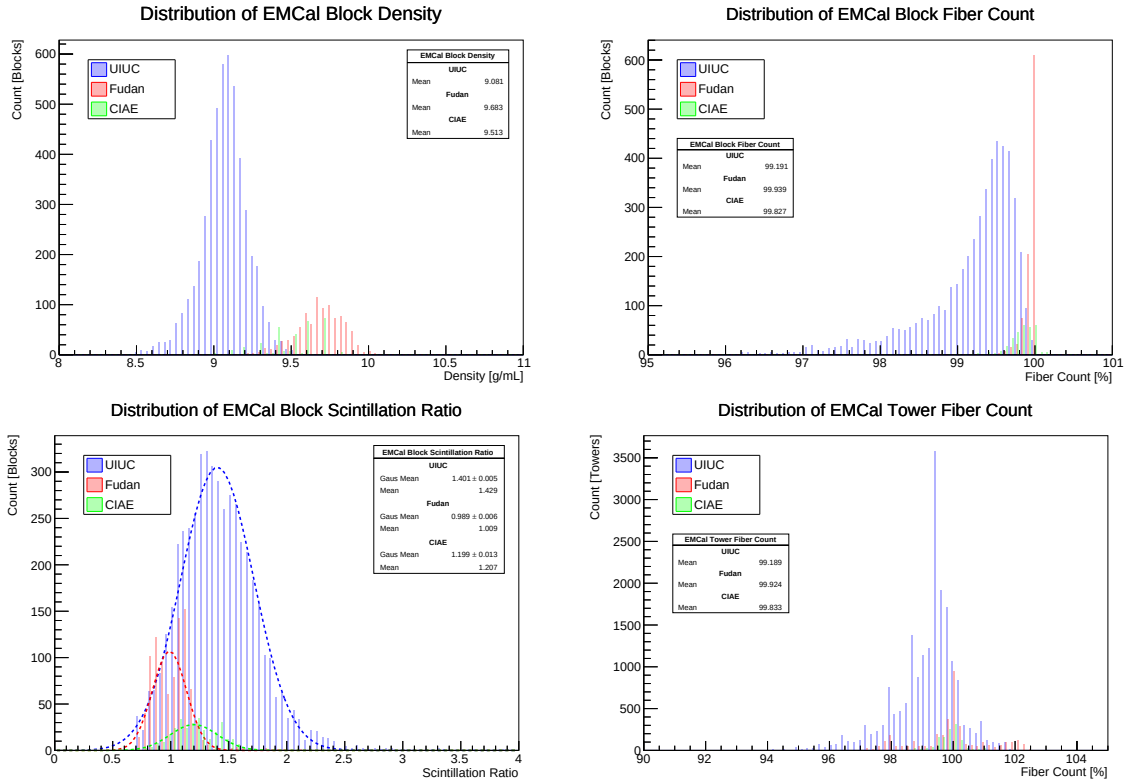

Figure 2.1: 1D distributions separately for UIUC and Chinese blocks. Left: distributions of block density (top) and scintillation ratio (bottom); right: distributions of light-transmission yield for entire blocks (top) and for towers (bottom).

2.2 Light-transmission yield and uniformity

In each block, the number of light-transmitting fibers was counted using a software program taking as input an image of the illuminated block ends [15] [16]. The result was determined for the entire block and also separately for each tower (quadrant) and represented as percentage of live fibers. The light transmission distributions are shown in Fig. 2.1.

2.3 Scintillation response

The scintillation properties of each block were measured by pulsing UV light through the block and recording the block's response (voltage) using a PMT. The threshold for a good block was determined relative to a calibration block at the time of the measurement and defined in [mV] [15] [16]. The result was represented as block response relative to the calibration block ("scintillation ratio" $U_{\text{block}}/U_{\text{calibration}-\text{block}}$). The distributions of scintillation ratio are shown in Fig. 2.1. It should be noted that (1) this test represents a qualitative confirmation that the fibers used in each block indeed have scintillation properties, but it should not be used in a quantitative manner, and that (2) the average UIUC scintillation ratio is not centered around 1 since the calibration block gave a consistently smaller response, which was stable over time relative to the tested blocks.

2.4 UIUC database

During EMCal block construction and testing at UIUC, a database (google sheet) was compiled including various properties for each block [22]. Each block was assigned a unique static traveler number called DBN (Data Base Number). The two main master tabs in the UIUC database are called `Blocks DB` for S1-12 blocks, and `Blocks1364DB` for S13-64 blocks [12]. Into these two tabs most of the raw information was filled on a day-by-day basis ordered by DBN in the historical order the blocks were produced, with one row per block. There are in total 103 columns in each of the master tabs providing the following pieces of information: general (columns A-H, CM), fibers (I-N), tungsten powder (O-W, CR), epoxy (X-AD), machining (AE-AG), dimensions (AH-AT, CS-CY), LT testing (AU-BM), scintillation testing (BN-BR), photo testing (BS-BT), testing cross checks (BV-BX), testing dates (BZ-CB), block grades (CC-CL), and location of block in sector (BU, BY, CN-CQ). Due to the high volume of manually managed data, two google script interfaces were created: one interface to quickly retrieve information about a block, or a group of blocks, and one interface to enter data for a group of blocks [17]. The latter significantly decreased the number of human mistakes: on a typical workday, several users had to enter various pieces of information for in average 12 blocks. A flow chart of the UIUC DB is provided in Fig. 2.2.

The used materials and the test results of blocks produced in China were compiled in excel sheets [23], which were sent to BNL and UIUC. The data of the Chinese blocks were entered into the UIUC database in the separate tab `FudanDB`. The quality of the Fudan and CIAE / PKU blocks was assured before shipping the blocks to BNL in tests similar to those carried out at UIUC, including an additional "AA" grade for blocks with no more than $0.1''$ dimensional deviation, block density within (9.5 ± 0.5) g/cm^3, LT $\geq 99\%$, LT-tower $\geq 97\%$, and otherwise as in Tab. 1.2. "C-grade" blocks were considered failing.

The following conventions for DBNs were used:

- DBN<2000: UIUC blocks S1-12
- DBN≥ 2000: UIUC blocks S13-64

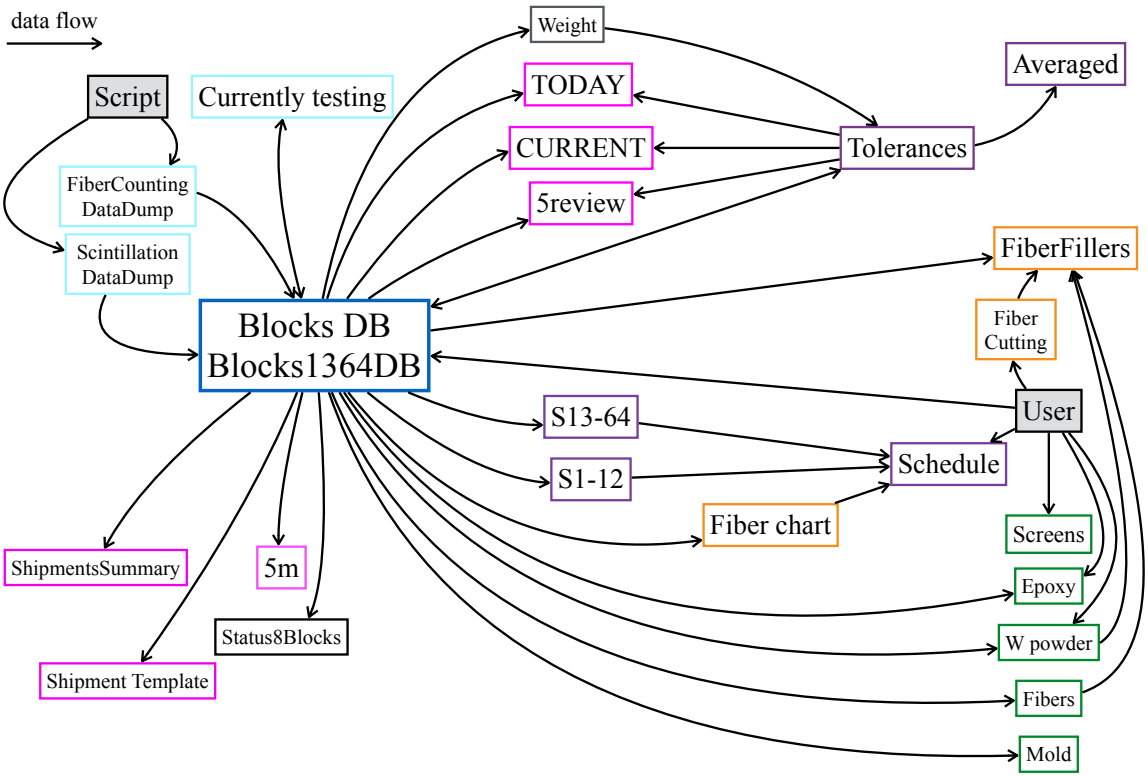

Figure 2.2: Data flow in the UIUC EMCal block database (google sheet) [22]. Each box represents a tab in the google sheet, arrows indicate data flow. Note that "sheet" refers to the entire document, "tab" to one tab within that sheet. The main master tabs `Blocks DB` and `Blocks1364DB` feed and retrieve data from various other tabs. Tabs in light blue provide the input testing data, those in light magenta and orange day-to-day overviews, those in dark magenta overall overviews, and those in green contain raw material overviews. Users updated the main tabs daily and some other tabs when required.

- DBN=FX, with X = 2- or 3-digit number: Fudan blocks
- DBN=CX, with X = 2- or 3-digit number: CIAE / PKU blocks

Examples are given in the caption of Fig. 2.3.

2.5 BNL DBN maps

The block (DBN) locations provided in the "travelers" of each glued sector with specific serial number were documented at BNL in excel sheets [24] [25], which were sent to UIUC and entered into the UIUC database [22]. While blocks made at Fudan (CIAE / PKU) were assigned DBNs of the form "FSX" or "FXX" ("CX") at the production sites and in the UIUC database (see also Sec. 2.4), with X a 2- or 3-digit number, the blocks produced in China were labeled 10,000 + X for Fudan blocks (12,000 + X for CIAE / PKU blocks) in the BNL travelers in order to have a set of purely numeric DBNs. The convention to assign each block a unique position in the 2-dimensional sector coordinate system is explained in Fig. 2.3.

		Sector 56		
	D	C	B	A
1	2554	2449	2446	2444
2	2495	2468	2404	2462
3	2608	2604	2556	2543
4	5858	5852	5827	5817
5	5792	5774	5754	4310
6	5734	5713	5709	5697
7	5676	5667	5664	5656
8	5632	5594	4463	4000
9	5579	5562	5541	4549
10	5873	5485	4582	4565
11	5474	5465	5440	5432
12	5413	5378	4708	4704
13	4788	4757	4754	4741
14	5315	5297	4845	4818
15	5266	4895	4873	4863
16	4929	4934	4917	4914
17	5159	4988	4985	4970
18	5123	5092	5075	5058
19	12217	12196	12192	12135
20	10956	10867	10840	10836
21	10963	10931	10907	10848
22	10917	10915	10895	10858
23	12265	12232	12173	12153
24	12272	12266	12256	12250

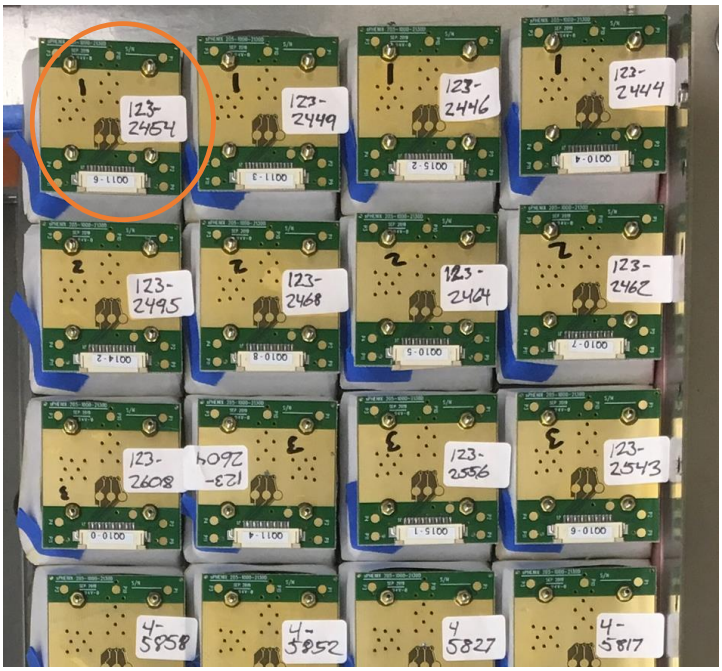

Figure 2.3: Left: demonstration of convention for EMCal block positions ("travelers") for one EMCal sector. When the sector is sitting on the assembly table with the saw teeth underneath the blocks, and thus looking at the narrow block ends, the blocks are labeled DCBA from left to right and 1-24 from top to bottom. Right: photo of the same sector (56), zoomed to blocks 123 and 4, with labeled PCBs attached to the narrow end (the labels were removed after the blocks were epoxied). For example, the circled block in the photo is **S56D1** and has DBN 2554, a UIUC S13-64 block. S56A24 is DBN 12250 (or C250), a CIAE/PKU-block, and S56B21 is DBN 10907 (or F907), a Fudan-block. To obtain the representation as in Fig. 1.7, the sector (in that figure) has to be rotated clockwise by 90°, and the area marked by the red box corresponds to block A1 (readout channels 60-63), here DBN 2444.

During block production, and during block inventory at BNL, it happened multiple times that DBNs were misidentified (for example, because of bad handwriting or typos), thereby introducing troublesome **double DBNs**. Due to careful double checks, most of the double DBNs could be caught before the blocks were shipped to BNL, but some slipped through or were introduced at BNL. The final list of problematic DBNs resolved between the production sites and BNL is compiled in Fig. 2.4, leaving only one pair of possibly swapped blocks. The BNL traveler sheets [24] [25] reflect only some of the changes indicated in Fig. 2.4, but all changes have been taken into account in the UIUC database and thus in the sector maps in Sec. 3. The map of DBNs is shown in Fig. 2.5, together with a map visualizing the block production dates (potting dates for UIUC blocks, machining date for Fudan/CIAE/PKU blocks).

					1. **Resolve** blocks with wrong BL - easiest = "likely correct"				
					2. Then **assign** DBNs for paired BL if possible using Sean's photos, if not, then FIFO system.				
Known double+ DBNs:					wrong BL type				update 20220715 (from 20220517 Sean file)
	BL-DB	pos1	pos2	pos3	resolved	corr2	corr1	remark	assumed = based on shipment date
1356	123	S9C2	S27D6		?	4356 (BL 6)	-	assumed in DB. is 4356?	
2204	123	S20A5	S32D1		?	-	2704	assumed in DB (correct BL 5)	
2404	123	54B2	56B2		?	2464	-	corrected in DB	confirmed by Sean
2554	123	55D2	56D1		?	2454	-	corrected in DB	confirmed by Sean
2811	7	S23A7	S24A7		?	2841	-	assumed in DB. is one 2841?	no solution offered by Sean. Both sector numbers and shipping dates (relatively early) are close to each other, so it is not possible to say which is which and we just assign.
3484	16	S17D16	S26C16		?	3487	-	assumed in DB. is one 3487?	assumed correct by Sean
3516	15	S27D15	S41D15		?	3546	-	assumed in DB. is one 3546?	assumed correct by Sean
3565	15	S21D15	S31B15		?	3569	-	assumed in DB. is one 3569?	assumed other way around by Sean, corrected in our DB
4316	5	52D14	46D5		?	-	5316 (BL 14)	assumed in DB. is 5316? (is correct BL 14)	
4381	6	S38D6	S47D10		?	4581 (BL 10)	-	assumed in DB. is 4581? (is correct BL 10)	
4538	9	S29A9	S47C9		?	4548	-	assumed in DB. is one 4548?	assumed correct by Sean
4547	9	38D9	57B6		-	4347 (BL 6)	-	assumed in DB. is 4347 (correct BL 6)?	
4717	12	49B12	36C12		?	-	4714	corrected in DB	confirmed by Sean the other way around, corrected in our DB
4813	14	42C14	61D14		?	4815	-	assumed in DB. is one 4815?	assumed correct by Sean
4936	16	61D16	58C16		?	-	5906	assumed in DB. is one 5906?	4936 assumed to be correct by Sean, no solution offered for the other one. I assume the one in S61 is 5906 - this block is not claimed, has the same BL (16) and the 2 digits that are different may have been read wrongly?
5341	13	53D6	46D13		?	-	4341 (BL 6)	assumed in DB. is 4341? (correct BL 6) possible also 4356	
5463	11	55B11	61B11		?	5462	-	assumed in DB. is one 5462?	assumed correct by Sean
5474	11	60B10	56D11		?	-	5494 (BL 10)	assumed in DB. is 5494? (correct BL 10)	
5632	8	53A11	56D8		?	-	4632 (BL 11)	assumed in DB. is 4632? (correct BL 11)	
5645	7	53A7	61D7		?	-	5695	assumed in DB. is one 5695? any relation to 5690?	assumed correct by Sean
5647	7	50C8	61C7		?	-	5617 (BL 8)	assumed in DB. is 5617? (correct BL 8)	
5655	7	61B7	61D8		?	5595 (BL 8)	-	assumed in DB. is 5595? (correct BL 8)	
5838	4	55A15	60C4		?	-	5238 (BL 15)	assumed in DB. is 5238? (correct BL 15)	
5875	18	53A18	57A6		?	5878 (BL 6)	-	assumed in DB. is 5878? (correct BL 6)	
F82	19	S14A19	S16C21		yes	F81		corrected in DB	
F693	20	S42A20	S42B21		yes	703		corrected in DB	
F793	22	49C22	45B21		?	F743 (BL 21)		assumed in DB	
F883	20	45A20	60B20		?		F833 (BL 20)	assumed in DB	assumed correct by Sean
F768	24	53A24	46A22		yes	F758		corrected in DB	
C183_1	19	54C19	53C24		yes	C183_2		is a true double DBN - BL 19 and BL24. I labeled them C183_1 (BL 19) and C183_2 (BL 24)	

Known other problems		likely correct	resolved	possible / assumed
Position	DBN	correct?		
40D10	~~5447~~	5497	is S40D10 but block was shipped only Nov 2, 2021, long after the sector was glued	
36C2	~~22455~~	2455	assumed in DB. 5-digit DBN	
51C15	4857	? (could be OK)	is 51C15 but Sean and I had agreed to fail that block (group 3 in Jan 2022). Could just be that he yet used that block, fine.	
26D16	3492	? (could be OK)	is glued in early Sector (26) in group 3 in late 2021 and should be failed, actually	
64C14	5923	4823?	assumed in DB. 5923 is a fiber set!	
11C5	1250	1205 is dummy?	is also a block in a dummy sector?!	
09B24	739	759 is dummy?	is also a block in a dummy sector?!	
08D14	938	958 is dummy?	is also a block in a dummy sector?!	
13B21	~~1005~~	10055	assumed in DB. was marked in Sean's sheet from 5/4/2021 as F55 and later likely a typo was introduced	
03B1	241	242 is dummy	is also a block in a dummy sector?!	
09B13	967	907 is dummy	is also a block in a dummy sector?!	
12D17	864	869 is dummy	is also a block in a dummy sector?!	
62C7	~~6678~~	5678	is assumed. would be correct block type. Check if claimed later.	

Figure 2.4: List of resolved problematic DBNs. The grass-green rows are confirmed (based on photos or direct visual inspection), the green-blue rows are very likely correct (based on previously wrong, now correct BL type), and the magenta pairs of DBNs are assumed to be correct based on the block shipping dates and assuming a "FIFO" system. The only truly questionable pair of blocks is [2811 (S23A7), 2841 (S24A7)] with very close shipping dates, for which positions may be swapped in reality. The DBNs of blocks that were shipped to BNL but not glued into sectors are: 286, 4956, F11, F929, F945, C234, C244, and C262.

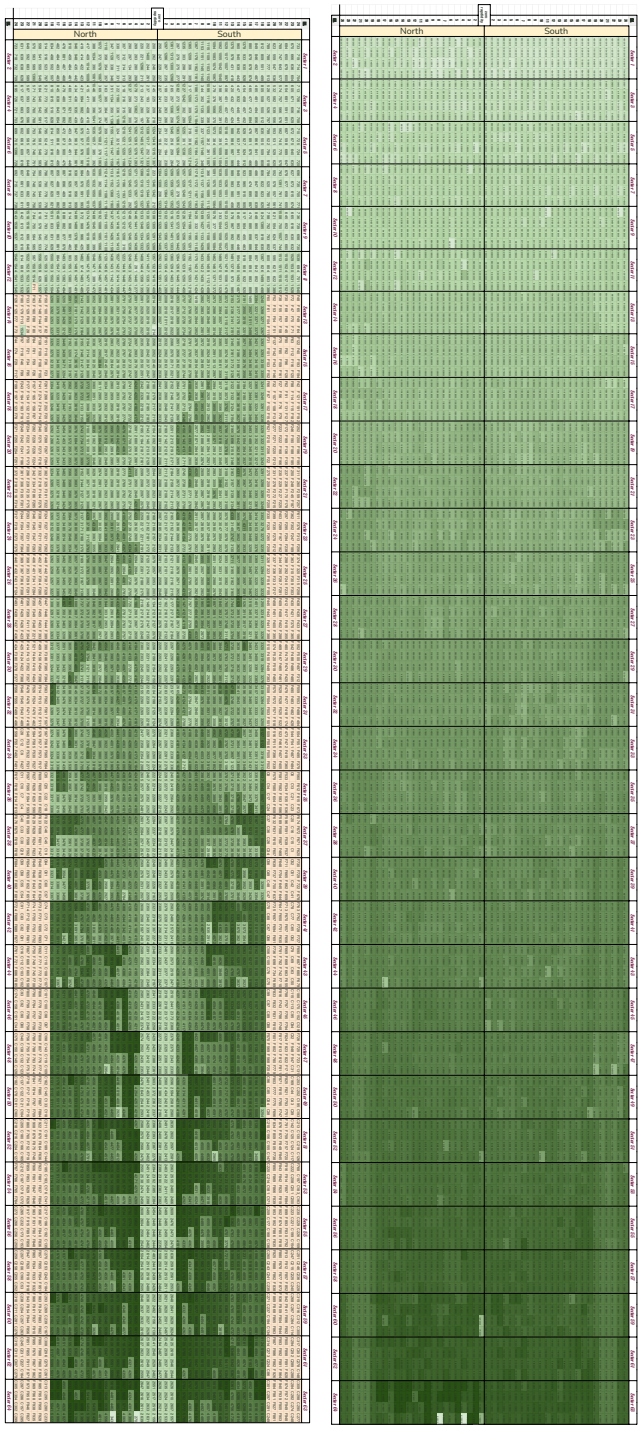

Figure 2.5: (zoom in online) EMCal map of DBNs (left) and production dates (right, between April 2019 and February 2022) with the cylinder of all 64 sectors cut open and rolled out on the plane. One box with thick black line represents 1 sector with 96 blocks each. The sectors are ordered by their serial numbers, which do not represent the actual physical location. South (North) sectors with odd (even) numbers are on the right (left).

2.6 Cosmic MPV

Each completed sector was tested between 2021 and mid-2022 in a cosmic-ray test stand at BNL as schematically shown in Fig. 2.6. From the measured ADC distributions, the **mean probable value**

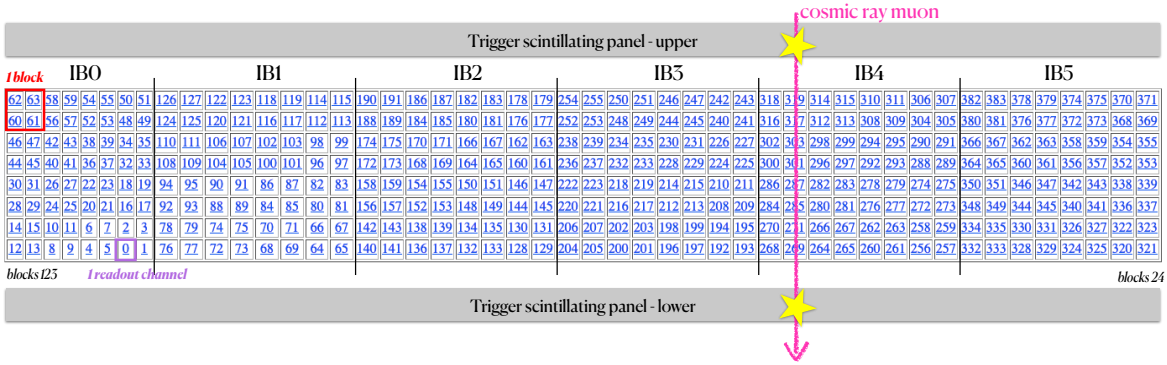

Figure 2.6: Schematics of cosmic test stand for one EMCal sector.

(MPV) was extracted for each ADC channel. The extraction sequence is detailed in Fig. 2.7, which also shows for one example sector the MPV vs. channel and vs. block distributions. The MPV is proportional to the energy measured by that ADC channel when the cosmic muon was passing through it. To translate this "precursor" of muon energy into a physical value in units of GeV, the ADC channel has yet to be calibrated, which is beyond the scope of this document (but an outlook is given at the end of this section).

The MPV and other distributions obtained from the pre-beam cosmic data taking at BNL are available on a BNL webpage [26]. The data are stored by 1 `*.root` file per sector on SDCC [27] and are processed with a `root` macro to produce histograms and the plots on the webpage [26]. The webpage offers a tag `physics` attached to some of the taken runs, which allows to determine which of the runs can be used for analysis. The output histograms are also available on SDCC [27]. For some ADC channels, no MPV values are available. These failing channels are attributed to poor angular coverage and not to intrinsic issues.

The MPV distributions are shown in Fig. 2.8. During the systematic analysis of the pre-beam cosmic data it was quickly realized that the type of used scintillating fibers has a significant impact on the average MPV - not only was the average MPV for blocks filled with Kuraray fibers found to be higher by about 60%, but also was a difference found between blocks built with the early Saint-Gobain batches delivered to UIUC and those built from the later batches, as summarized in Tab. 2.1 and Fig. A.1. This variation

Table 2.1: MPVs split up by used scintillating fibers from the suppliers Saint-Gobain (SG) and Kurary (K), and block production site. All UIUC blocks were made with SG fibers, which were delivered from Saint-Gobain to UIUC in two different periods: the S1-12 fiber purchase order (PO) had delivery dates between July and November 2018, and the S13-64 PO between April 2019 and February 2021. The MPV averages and the MPV statistical uncertainties for the block sets were propagated according to Eqs. 4.1 resp. 4.2.

fiber type	average MPV	block count
UIUC S1-12	265±12	1158
UIUC S13-64	319±7	3718
China HS-SG	387±8	695
China K	509±11	546
all SG	316±8	5599

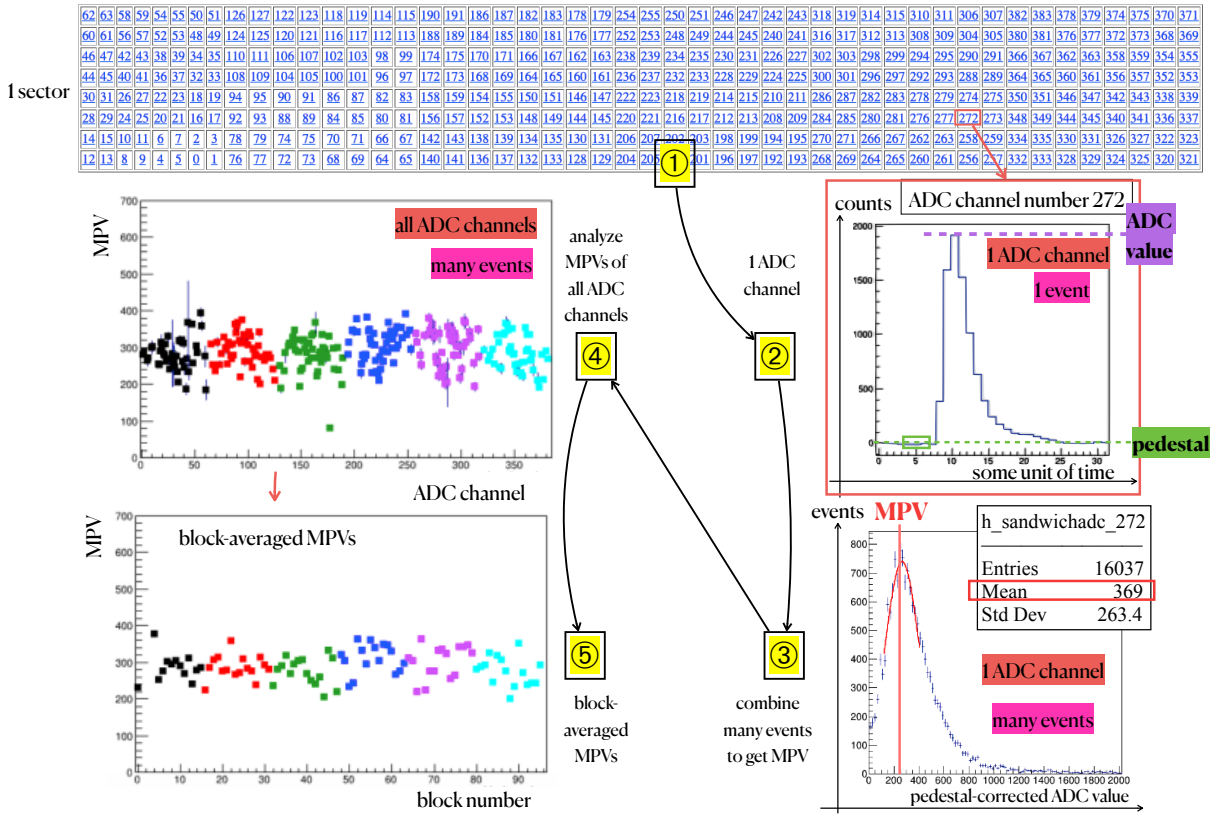

Figure 2.7: MPV extraction sequence starting from a full sector ① and then picking ADC channel 272. ② The **ADC value** (or **ADC count**) for a given ADC channel and given event is determined as the height of the peak in the timing spectrum for that ADC channel. The **pedestal** is the average count offset from 0 in a certain range as indicated by the green box. (The shown histogram is already pedestal corrected, which is why the green dashed line is at 0.) ③ Many ADC values from different events (*), but for the same ADC channel are combined and the resulting distribution is fit by a Gaussian function. The mean of the Gaussian fit is the "mean probable value", or **MPV**, of that ADC channel. ④ The MPVs are recorded for each ADC channel and ⑤ 4 channels are averaged to obtain the MPV on block level [26]. The uncertainties are taken from the error on the Gaussian fit (see also Sec. 4.2). (*) The histogram `h_sandwich` is filled only for events for that the channels above and below the given channel measure a peak height of > 100 counts.

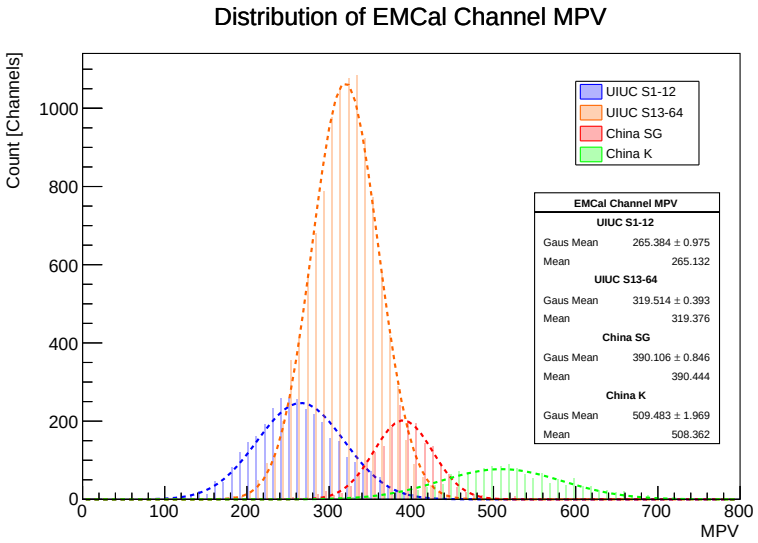

Figure 2.8: MPV distributions (one entry per ADC channel = tower) for UIUC and Chinese blocks. The UIUC blocks are shown as two separate samples: for the early ("S1-12") fiber batches 1-A through 16-B and the later fiber batches 21-A through 68-C ("S13-64"), see also App. A.

between UIUC and Fudan/CIAE/PKU blocks, and the variation within UIUC blocks, will be discussed in the following.

Higher block density? Since the absorber density ρ enters the Bethe-Bloch formula linearly, $\mathrm{d}E/\mathrm{d}x \propto \rho$, one could be tempted to attribute the effect of higher average MPV of Fudan/CIAE/PKU blocks made with SG fibers as compared to UIUC blocks to the higher density of Fudan/CIAE/PKU blocks. The ratio between Fudan/CIAE/PKU and UIUC average MPVs is however quite larger than the corresponding ratio of the block densities[1], with $\langle\mathrm{MPV}\rangle$(HS-SG) / $\langle\mathrm{MPV}\rangle$(HCS)=1.26±0.04, while $\langle\rho\rangle$(HS-SG) / $\langle\rho\rangle$(HCS)=1.05.

Different SG fiber production cycles? The SG fibers used in China were shipped from Saint-Gobain to UCLA, from where they were forwarded to Fudan University. Delivery to UCLA started in early 2021, at the end of the delivery period for UIUC S13-64 fibers. It is therefore not excluded that the SG fibers used in China stem from a different production cycle at Saint-Gobain. Interestingly, UIUC used one SG fiber batch that had originally been ordered for the Chinese collaborators ("UIUC batches 67 and 68"). The average MPV for blocks made from this batch is 323, consistent with the SG S13-64 average, and significantly smaller than the Fudan/CIAE/PKU SG average, thus not supporting the idea that the SG fibers ordered for the Chinese production provide per se a higher cosmic muon response.

Higher light-transmission yield? As shown in Fig. 2.1, the Fudan/CIAE/PKU blocks tend to higher fiber counts than the UIUC blocks, thus providing more fibers in average to collect yield in the cosmic ray test stand. While this may be one contributing factor to the differences in cosmic MPV observed between UIUC and Fudan/CIAE/PKU blocks, it is likely not the only one: anticipating the correlation between

[1] UIUC used HCS tungsten powder without exception, and only HS tungsten powder is considered in the calculation of the Chinese average in Tab. 2.1 to have a more uniform set of blocks.

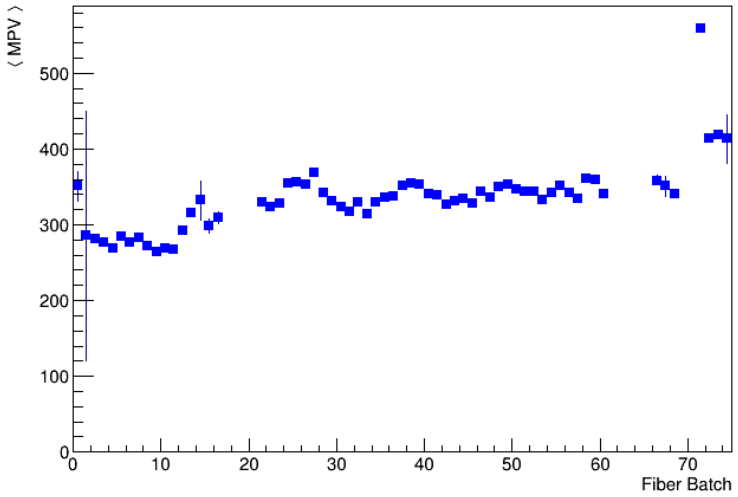

Figure 2.9: Average MPV versus fiber batch. UIUC used only fibers from Saint-Gobain (SG) and assigned batch numbers 1-68 plus a letter (A, B, C). In the figure, UIUC batches with same number but different letters were merged. UIUC batches 1-16 were mostly used for S1-12 blocks and UIUC batches 21-68 for S13-64 blocks. Batches > 70 were assigned to fibers used for the Fudan/CIAE/PKU blocks: 71 for Kuraray (K) fibers, 72 for SG fibers sent from UCLA to Fudan, 73 for a initially bent batch of SG fibers plus K fibers ordered at CIAE and used at Fudan, and 74 for a small mixed sample of SG fibers ordered at CIAE and used at Fudan, plus K fibers. Batches 17-20, 61, 65, and 66 were not used (and are still available at UIUC), and batches 63 and 64 were sent to China for block production (and now appear in batch 72). Batches 67 and 68 were originally ordered for Fudan/CIAE/PKU blocks but were used at UIUC. See also App. A.

light-transmission yield and MPV in Fig. 2.11, the MPV values for UIUC blocks are well below those for Fudan/CIAE/PKU blocks also at the highest "LT" values of UIUC blocks.

In conclusion, there is at this stage no fully transparent explanation as to why the MPVs from blocks with SG fibers show such a large spread, other than Saint-Gobain fibers can vary greatly in scintillation response depending on their production batch. The cosmic MPV response is also found to vary significantly between producers (Saint-Gobain or Kuraray).

The purpose of this note is to document the variations in fiber response in order to pave the way for the first full calibration of the EMCal. A glimpse of an initial pre-calibration based (amongst others) on variations in fiber batches is given in Fig. 2.10. The correction results in a significant narrowing ($\sim 25\%$) of the ADC-channel distribution and a flattening of the distribution for the average cosmic MPV versus sector serial number.

2.7 Correlations between block properties

The measured correlations between properties on block- and channel-level are shown in Figs. 2.11, 2.12, and 2.13.

In Fig. 2.11, no correlation can be found between cosmic MPV and block density. Blocks with higher fiber

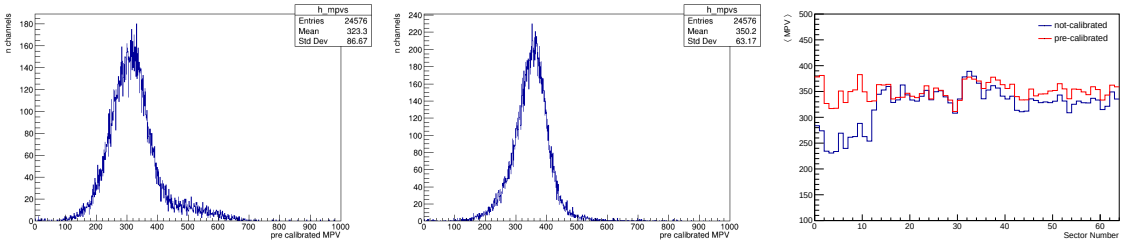

Figure 2.10: Initial pre-calibration of all EMCal ADC channels. Left: uncorrected MPV distribution; middle: corrected MPV distribution; right: average MPV versus sector serial number, with and without correction. The pre-calibration correction takes into account a) differences in single-pixel gaps between towers, and b) differences in fiber batches.

count trend to have a higher cosmic MPV. Also blocks with higher scintillation response (as measured at the producing institutions) trend to higher cosmic MPV values (as measured at BNL).

In Fig. 2.12, the correlation between scintillation response and fiber count is found to be positive for UIUC blocks and negative for Fudan/CIAE/PKU blocks.

The block quadrants and channels are mapped onto each other in Fig. 2.13 plotting the fiber count vs. the cosmic channel MPV. The correlations are less pronounced than on block level (see middle of Fig. 2.11).

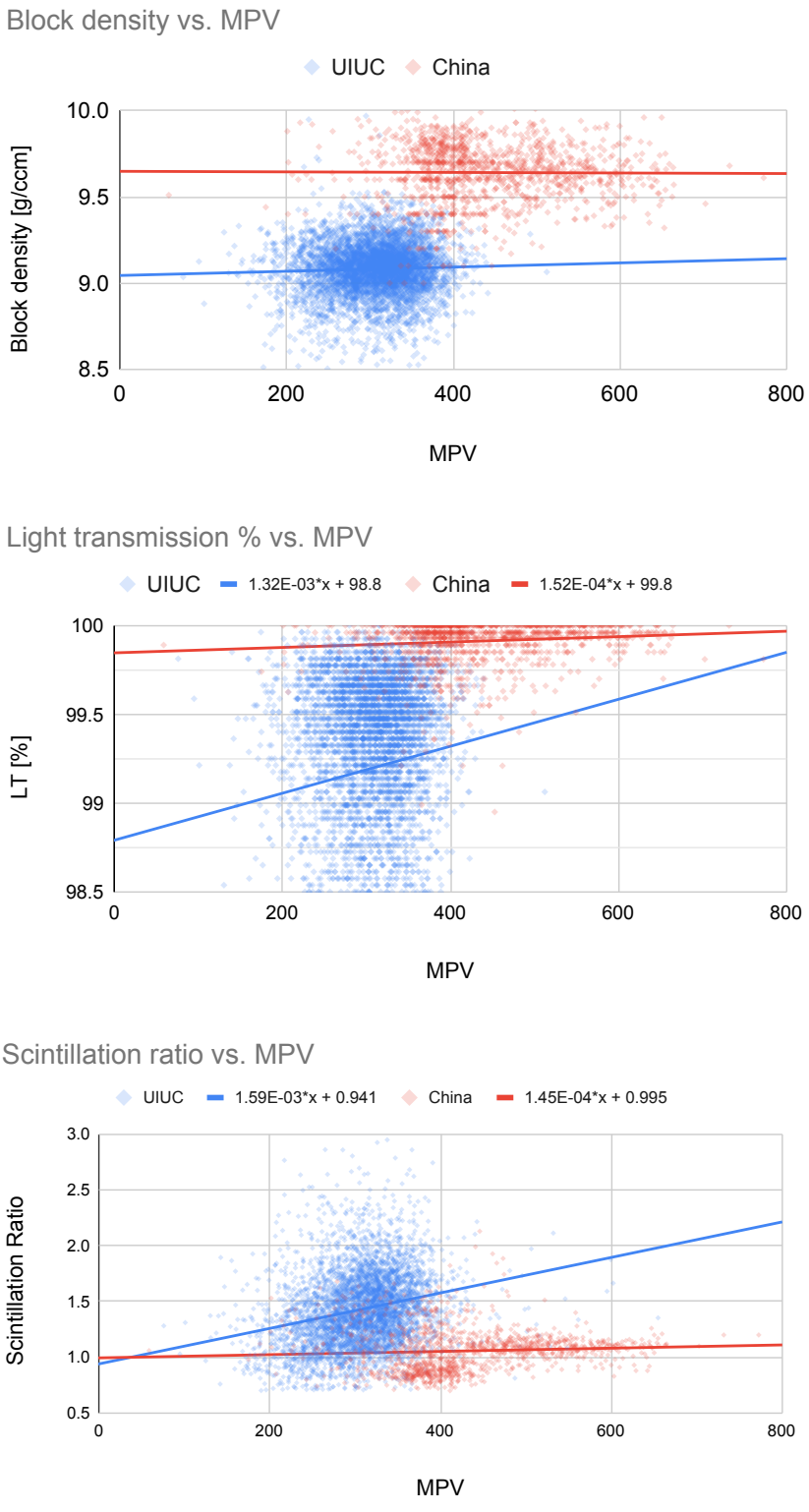

Figure 2.11: Correlations on block level between MPV and density (top), light-transmission yield (middle), and scintillation (bottom), separately for UIUC and Fudan/CIAE/PKU blocks.

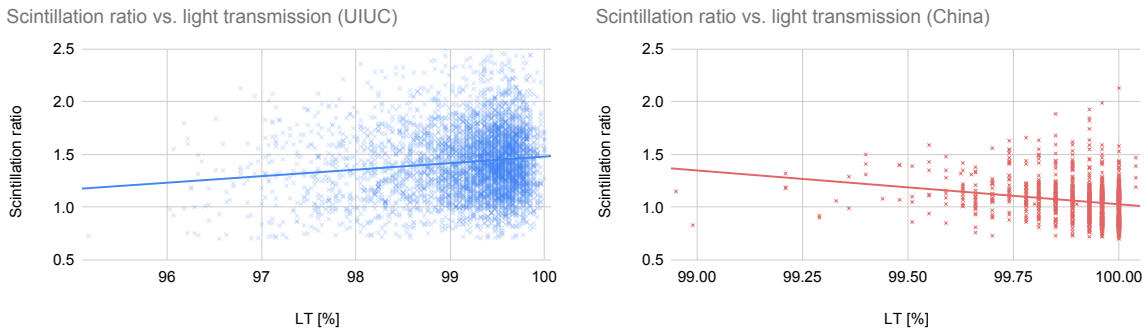

Figure 2.12: Correlations on block level between relative scintillation response and light-transmission yield, separately for UIUC and Fudan/CIAE/PKU blocks.

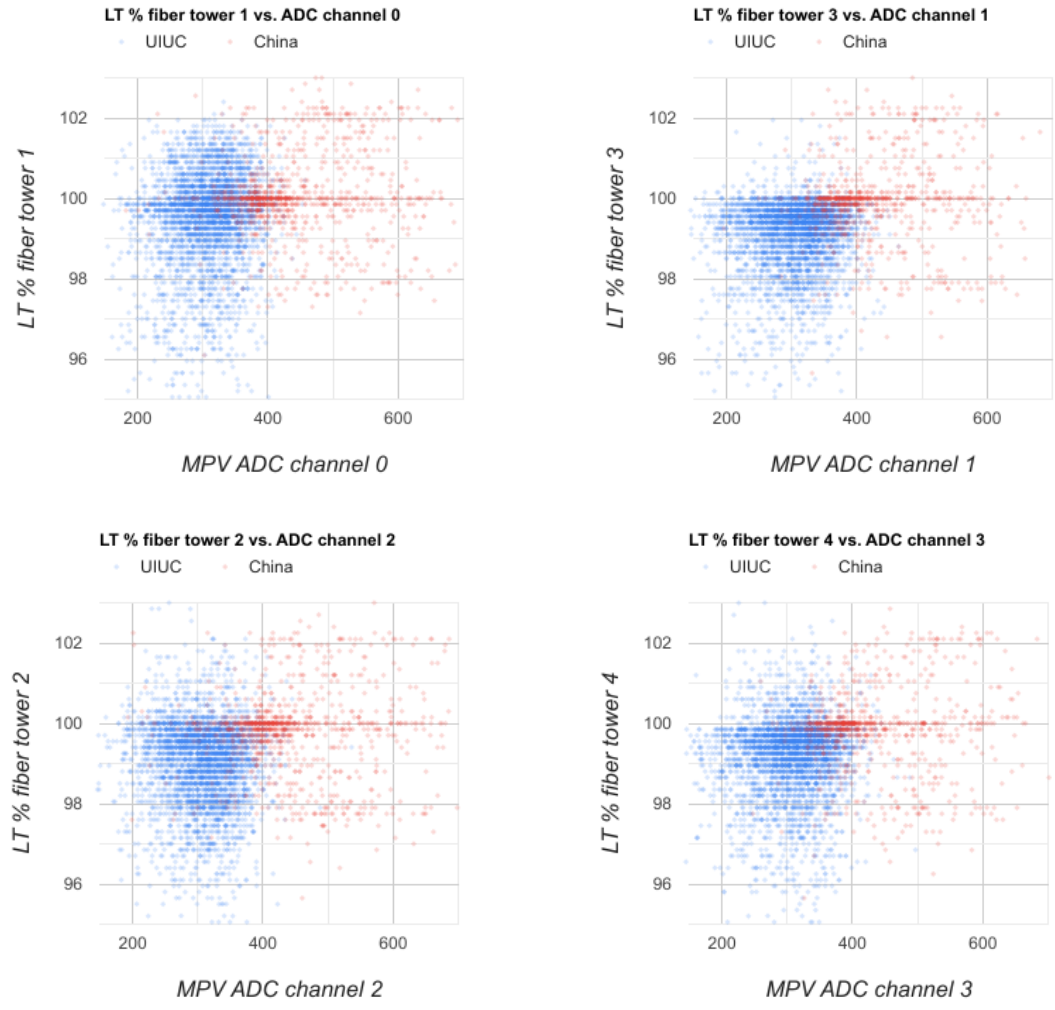

Figure 2.13: Correlations between ADC channel and fiber tower (light-transmission yield in quadrant), separately for UIUC and Fudan/CIAE/PKU blocks, mapping the corresponding ADC- and fiber-tower channels onto each other as defined in Fig. 3.1

3 Sector maps

An overview of the EMCal ordering scheme with respect to block positioning and channel numbering is given in Fig. 3.1. In the following, the EMCal cylinder will similarly to in Fig. 2.5 be rolled out flat, creating a 2-dimensional map with the horizontal axis representing the azimuthal angle ϕ and the vertical axis rapidity η. The South sectors are now in the top of the plane and the North sectors in the bottom. The horizontal mid-lines represent zero rapidity, and the top (bottom) edge horizontal lines highest negative (positive) rapidity $\eta \sim -1.1$ ($\eta \sim +1.1$), see also Fig. 1.1.

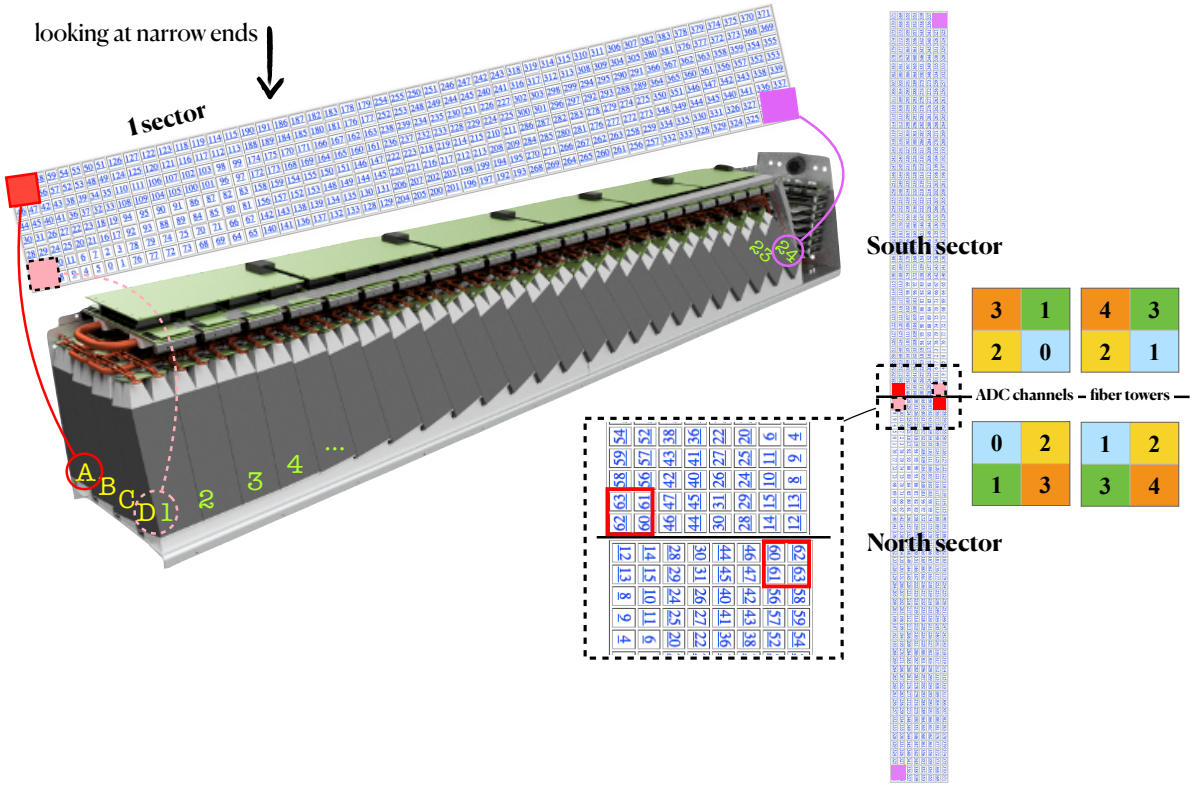

Figure 3.1: EMCal channels ordering scheme when looking at the narrow block (lightguide / SiPM) ends. The sketch on the left demonstrates the ADC channel numbering for one sector. The right hand side shows the ADC channels for a South and a North sector separated by the thick horizontal black line, where the North sector was flipped by 180° degrees so that blocks 123 meet at mid rapidity. Note that the numbering scheme for fiber towers (used in the light-transmission test, see Sec. 2.2) differs for historical reasons from that used for ADC channels and the mapping is provided here. Compare to Figs. 1.7, 2.3, and 2.5.

3.1 Maps ordered by sector serial number

The EMCal sectors were produced in a certain historical order (see Sec. 1.4) and each sector was assigned a **serial number 1...64**, where odd serial numbers were given to **South sectors** and even serial numbers to **North sectors**.

Note that while the blocks used in North and South sectors are identical, the geometry of an assembled North sector is such that it cannot be installed in the South portion of sPHENIX, and vice versa. The serial numbers do not reflect the actual physical locations the sectors will be installed in, the latter of which will be detailed in Sec. 3.2.

The EMCal maps ordered by sector serial number are shown in Fig. 3.2 for block density and light-transmission yield, and in Fig 3.3 for scintillation response and MPV. The labels on the x-axis (representing ϕ) correspond to the sector serial number, with the "DCBA" labels indicating individual blocks within a sector. The y-axis (representing η) displays the block types.

When ordered this way by sector serial numbers, the distinct S1-12 blocks, which were all produced at UIUC, become apparent in the left portion of the map. The S13-64 high-rapidity blocks (BL 19-24) were produced in China using materials from different suppliers or batches, which is reflected in the block properties (see also Secs. 1.4 and 2.6): higher block densities and higher MPVs.

Independently of the used materials, the light-transmission fractions are higher for the Fudan/CIAE/PKU blocks. Note that the relative scintillation responses between UIUC and Fudan/CIAE/PKU blocks cannot be directly compared since the UIUC average of the scintillation ratio is not at 1 (Sec. 2.3).

Figure 3.4 displays the cosmic MPV EMCal map (ϕ channel number vs. η channel number). The content in this figure is similar to that in Fig. 3.3, with the difference that the MPV is determined not with the **default sandwich triggering scheme** described in Fig. 2.7. Instead, a **one-sided trigger scheme** is used to identify towers triggered by cosmic muons: a veto is imposed on towers ± 1 in η and the energy deposit in the 4 towers following the sampled tower is selected. This modified triggering scheme helps populating the ϕ-edges of each sector. The gaps in MPV coverage with the default triggering scheme are visible in Fig. 3.3 as white entries. Figure 3.4 shows two versions of the MPV map: one default (=uncalibrated), and one with initial pre-calibration based amongst others on fiber-batch variations as described in Fig. 2.10. These maps are part of the set of KPP plots for the EMCal.

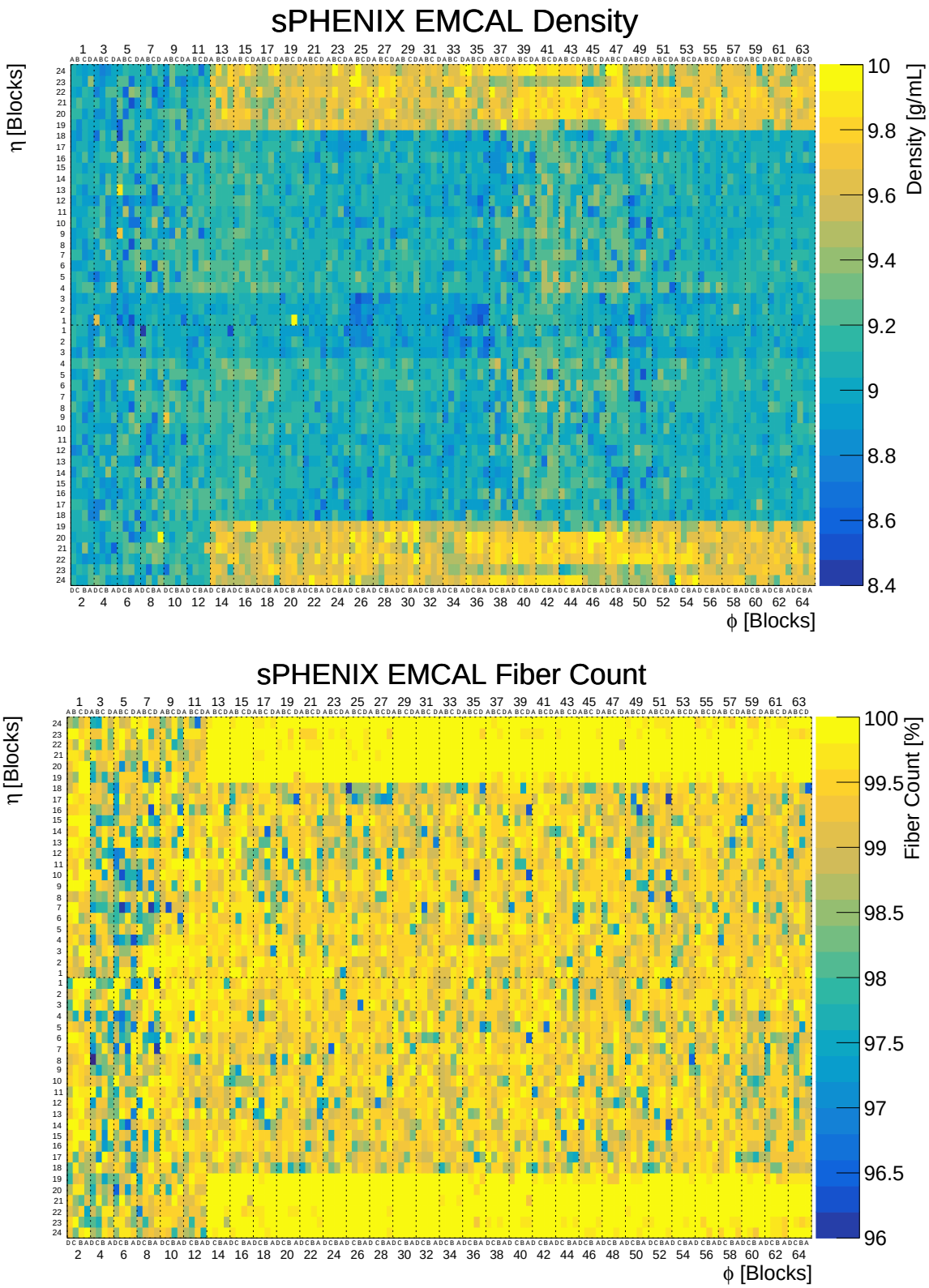

Figure 3.2: EMCal maps by sector serial number for block density (top) and light-transmission yield (bottom).

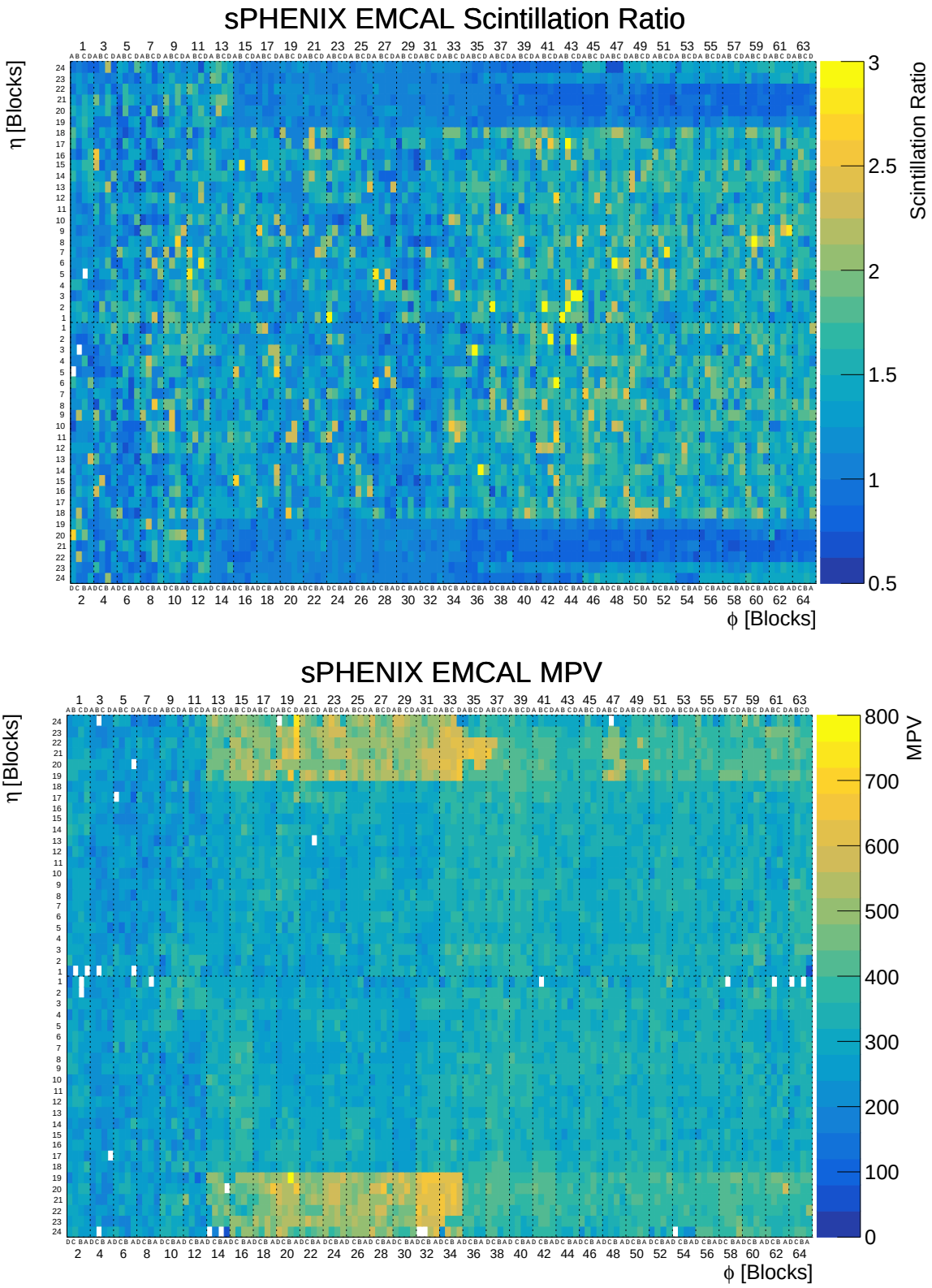

Figure 3.3: EMCal maps by sector serial number for scintillation response (top) and MPV (bottom).

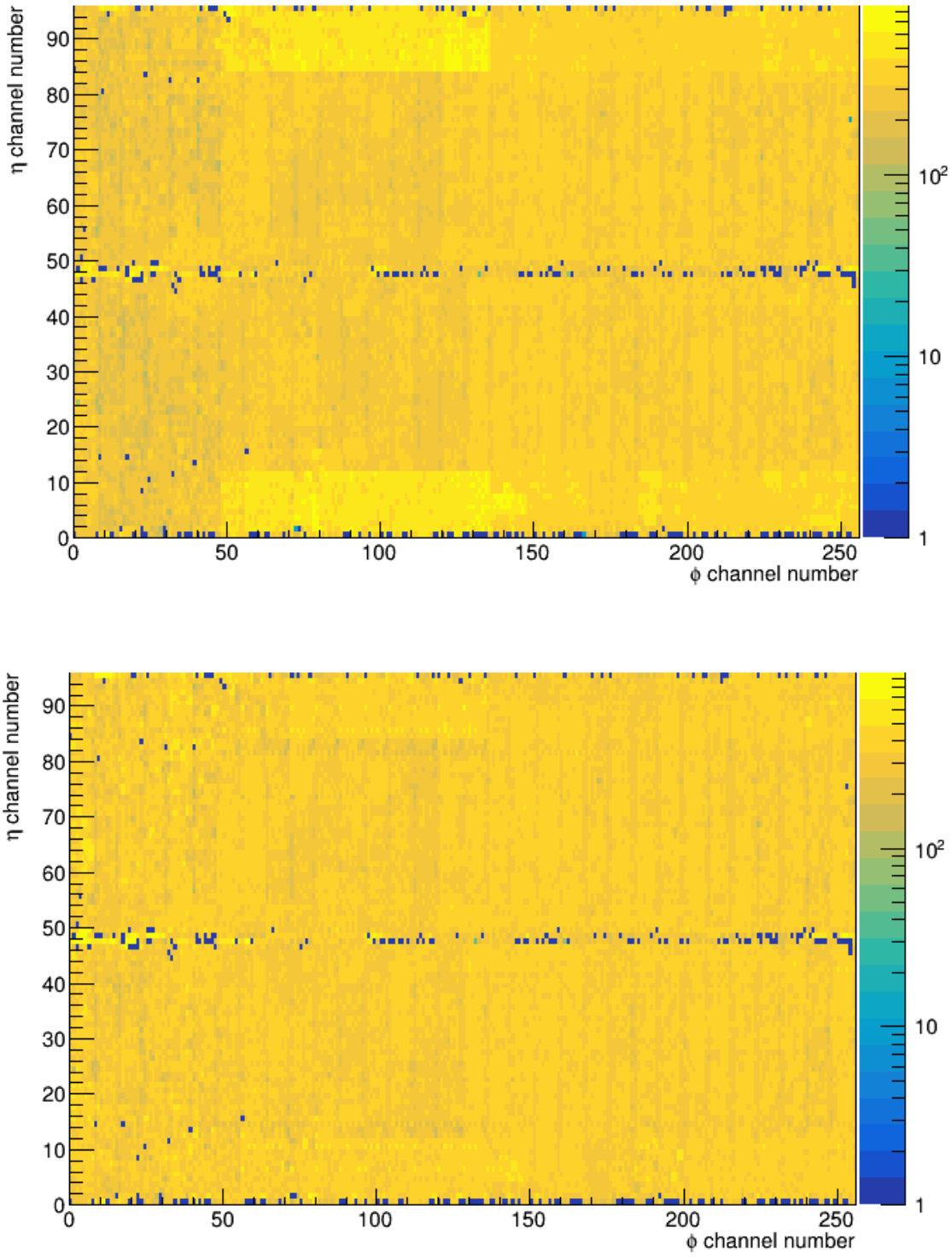

Figure 3.4: EMCal maps by sector serial number for MPV with modified trigger scheme to better populate the sector edges. Top: uncalibrated; bottom: with pre-calibration as described in Fig. 2.10.

3.2 Maps ordered by sector physical location

From the information contained in the maps in Sec. 3.1, each sector was categorized depending on its density and MPV of its blocks [28], both of which are features that affect the block response. The low-rapidity blocks (BL 1-18) were produced at UIUC throughout without change of material suppliers and the average MPV per sector is found to be stable, as shown in Fig. 3.5. Therefore the categorization of sectors was based on the MPV response of the high-rapidity blocks. As demonstrated in the figure, blocks BL 19-24 can be separated in three distinct groups: (A) UIUC Saint-Gobain fibers (Sectors 1-12); (B) China Kuraray fibers (Sectors 13-33); (C) China Saint-Gobain fibers (Sectors 34-64). Since the jump in block density coincides with that in MPV at S13, it does not provide any further constraints for categorization.

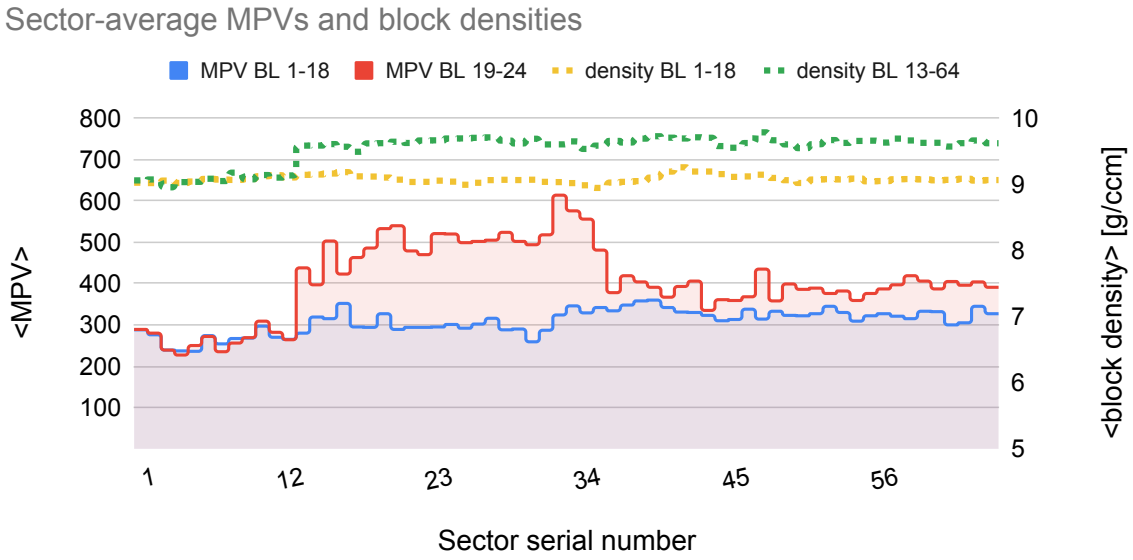

Figure 3.5: Average MPV and block density vs. sector serial number, split up for low- and high-rapidity blocks. Three categories are defined based on the jumps at S13 and S34.

In the distribution of sector serial numbers into physical locations, an approach was chosen that maximizes both North-South sector symmetries and azimuthal symmetries [28]. North- and South sectors were paired with minimal difference in average MPV. From the resulting 32 sector pairs, four groups were formed with low, mid, high, and very high average sector-pair MPV and the 32 sectors were distributed in azimuth such that no two neighboring pairs are in the same group, avoiding extended areas of very high or low average MPV, and such that pairs of similar average MPV are located point-symmetric in ϕ. For the reconstruction of $\Upsilon \rightarrow ee$ and other reconstructions for the heavy-ion program, a North-South symmetry is advantageous. In particular for the measurement of azimuthal transverse-spin asymmetries as part of the cold QCD program, a uniform response of the sPHENIX detector along the azimuth is needed to minimize false asymmetries, which blur the physics signal.

EMCal sector installation has not been completed at the time this note is written (August 17, 2022) and therefore the "physical maps" presented in this section have to be considered preliminary.

The mapping between sector serial and label numbers, physical location and ideal order of installation is shown in Fig. 3.6 and Tab. 3.1.

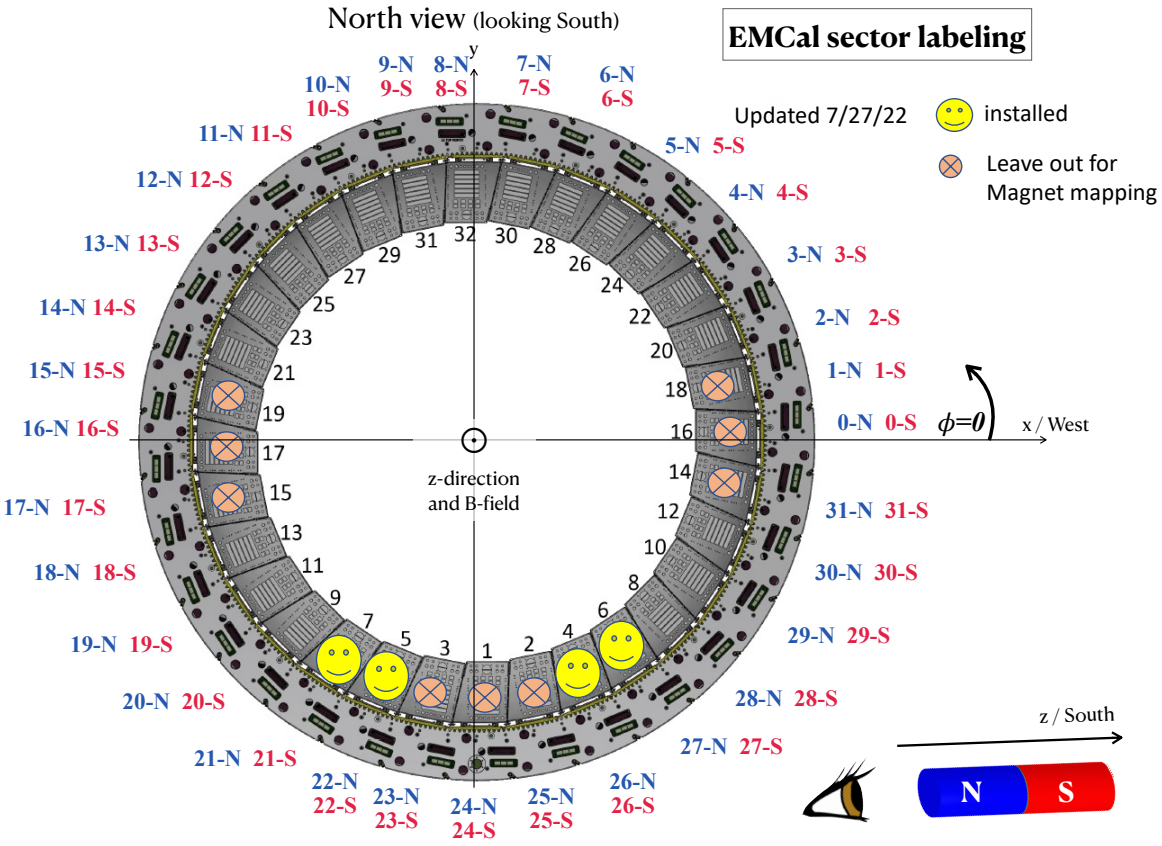

Figure 3.6: EMCal sector numbering schemes and locations. The black numbers inside the solenoid indicate the installation order of sectors, the blue numbers outside the sector labels for North (N) sectors and the red the sector labels for South (S) sectors. The mapping between label and serial numbers is given in Tab. 3.1.

Table 3.1: EMCal sector pairing, serial numbers (1...64), and labeling scheme used on the signal cables. For the latter, there are two sets of sectors (North / South) enumerated 0...31 starting with 0 at laboratory azimuthal angle $\phi = 0$ and then increasing with increasing ϕ [29] (see Fig. 3.6). Sectors are installed in N/S pairs and the pairing is indicated here including the ideal (but at the end of the day not carried out) order of installation. As shown in Fig. 3.6, sectors at 3pm (installation positions 14, 16, 18), 9pm (installation positions 15, 17, 19), and 6pm (installation positions 1, 2, 3) will be installed last to provide space for the magnet-mapping device. At the time this note is written, the sectors with serial numbers in bold have been installed into sPHENIX.

N serial	S serial	N label	S label	installation
4	7	24-N	24-S	1
2	11	25-N	25-S	2
54	45	23-N	23-S	3
22	**25**	26-N	26-S	4
46	**13**	22-N	22-S	5
30	**27**	27-N	27-S	6
18	**35**	21-N	21-S	7
56	**61**	28-N	28-S	8
36	57	20-N	20-S	9
34	21	29-N	29-S	10
32	33	19-N	19-S	11
40	47	30-N	30-S	12
14	17	18-N	18-S	13
52	55	31-N	31-S	14
64	63	17-N	17-S	15
12	5	0-N	0-S	16
6	9	16-N	16-S	17
44	49	1-N	1-S	18
60	53	15-N	15-S	19
42	37	2-N	2-S	20
38	41	14-N	14-S	21
20	19	3-N	3-S	22
24	31	13-N	13-S	23
58	51	4-N	4-S	24
50	59	12-N	12-S	25
26	15	5-N	5-S	26
28	23	11-N	11-S	27
62	39	6-N	6-S	28
16	29	10-N	10-S	29
48	43	7-N	7-S	30
10	1	9-N	9-S	31
8	3	8-N	8-S	32

Ordering the sectors according to their physical location results in the maps shown in Fig. 3.7 for block density and scintillation response, in Fig. 3.8 for the light-transmission yield, and in Fig. 3.9 for the MPV. Data for light-transmission count and MPV were recorded also on channel level and are shown both on block- and channel level. The switch between block- and channel level is detailed in Sec. 4.2. Figure 3.10 shows the MPV per channel in a lego-plot representation and also in cylindrical coordinates. Note that Figs. 3.7-3.10 resemble maps that are slightly out of date as of August 17, 2022: sector pairs (18, 35) and (26, 15) were actually swapped for practical reasons (and this is correctly displayed in Tab. 3.1).

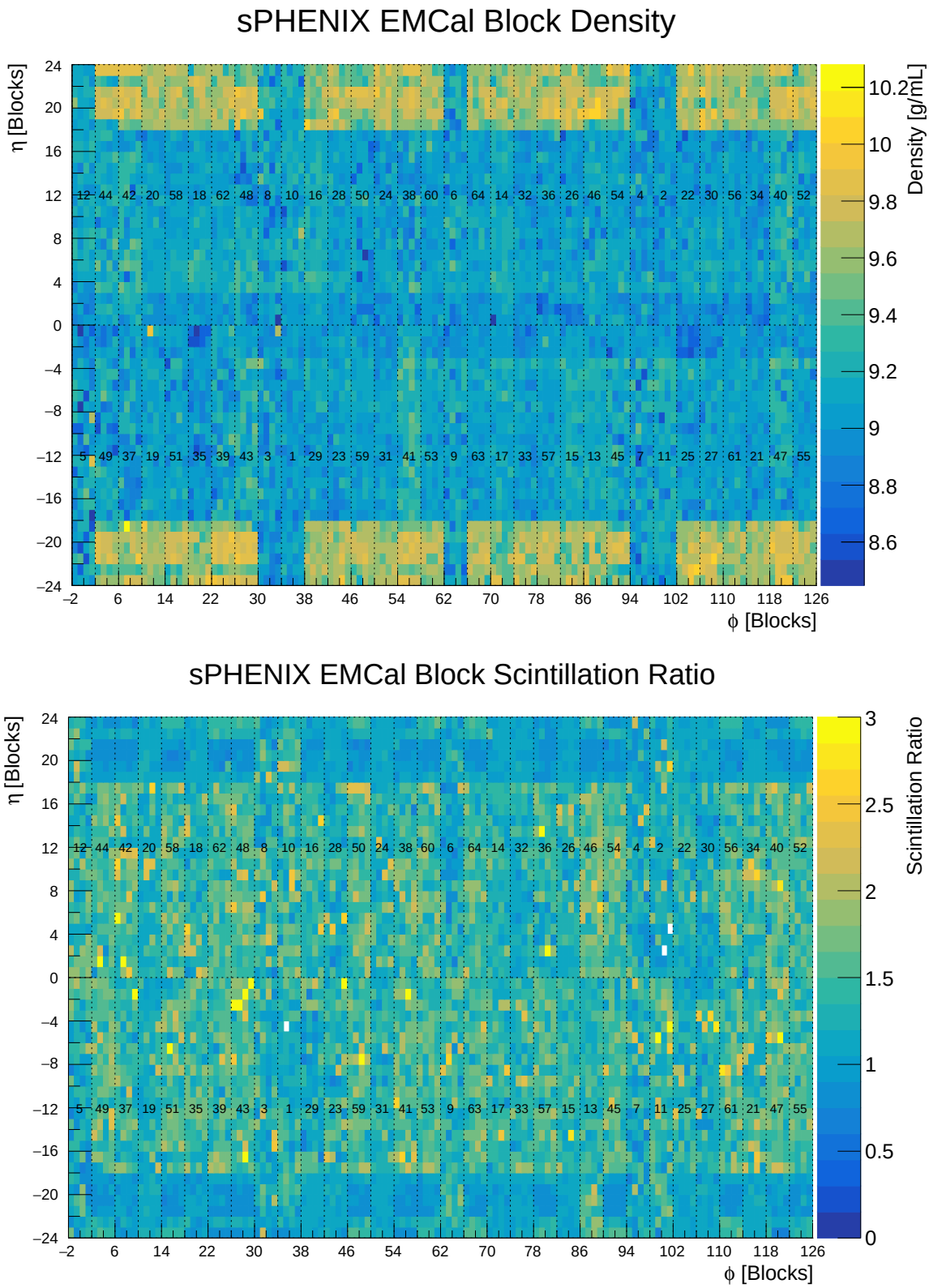

Figure 3.7: EMCal maps by physical sector location for block density (top) and scintillation response (bottom).

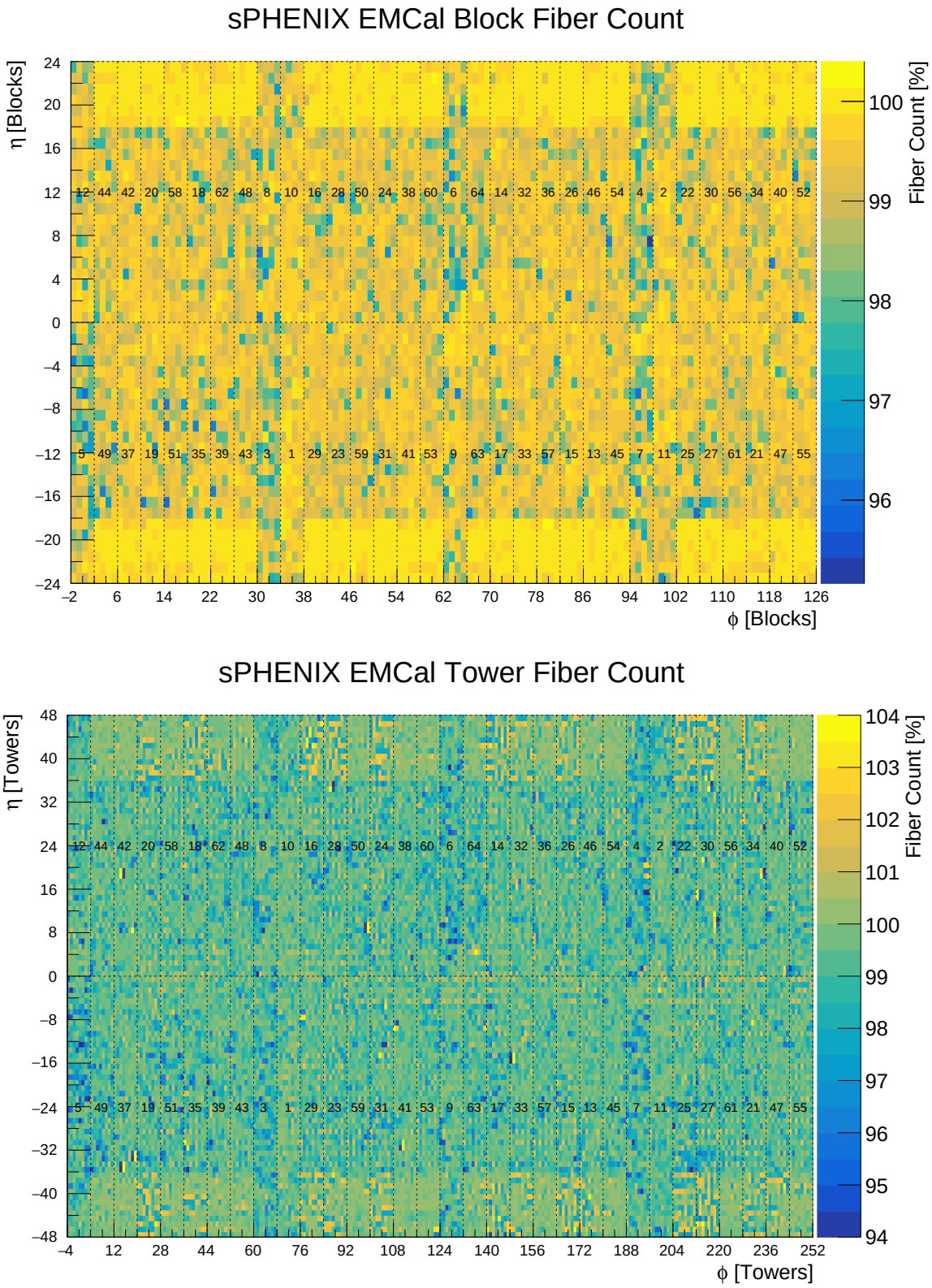

Figure 3.8: EMCal maps by physical sector location for block light-transmission yield on block (top)- and channel- (bottom) level.

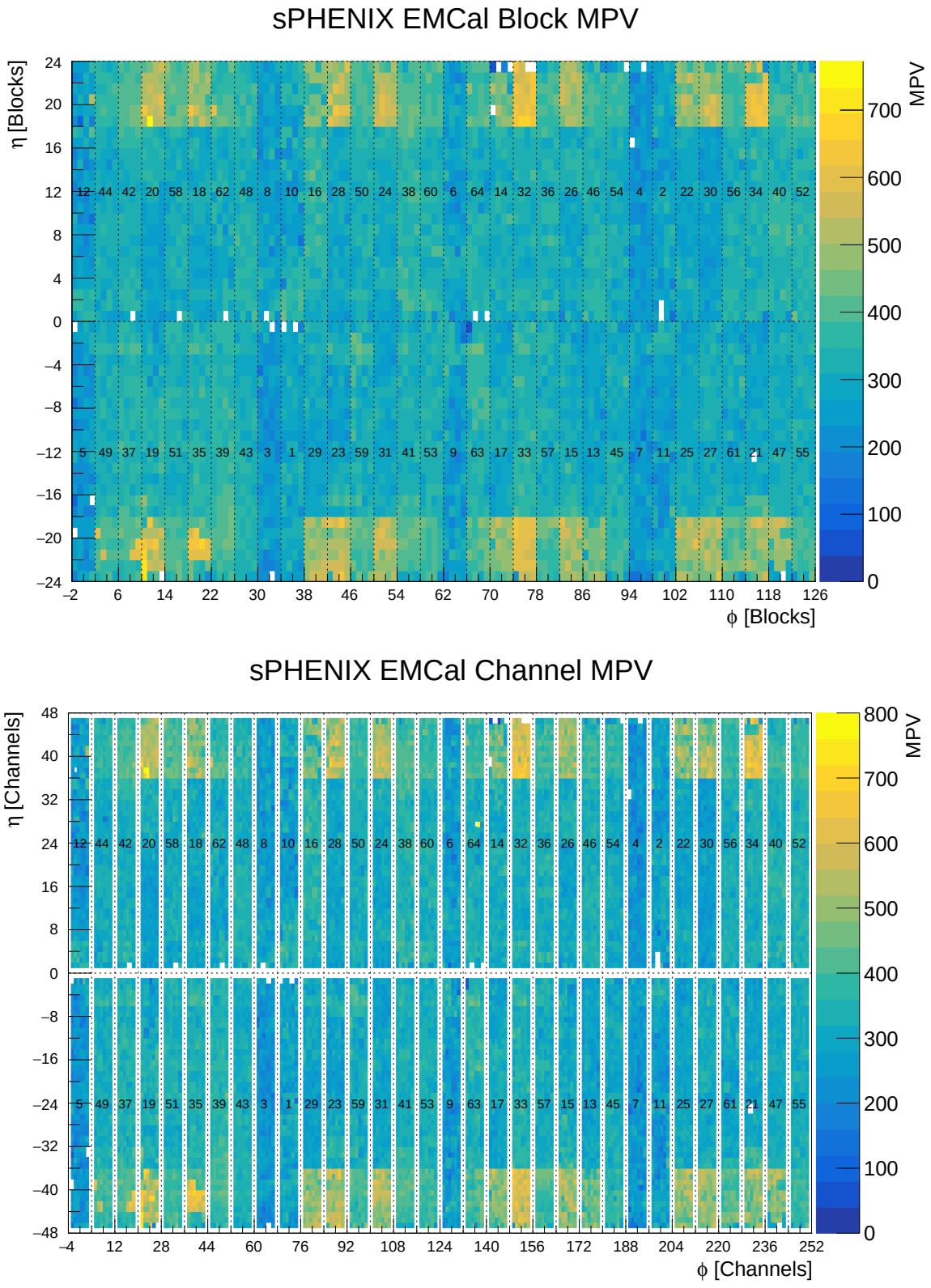

Figure 3.9: EMCal maps by physical sector location for block MPV on block- (top) and channel- (bottom) level.

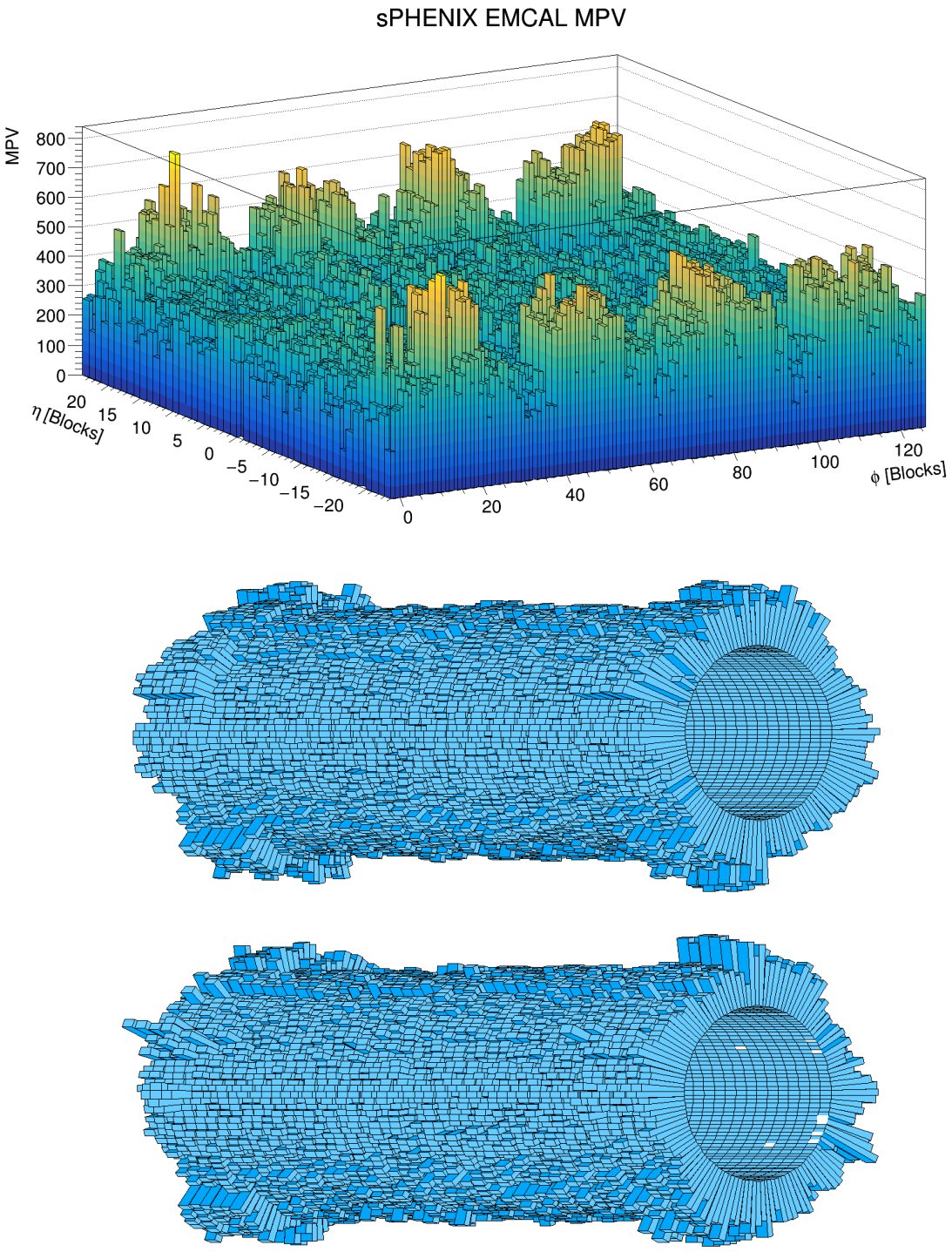

Figure 3.10: EMCal maps by physical sector location for block MPV on channel level, lego plot (top) and cylindric coordinates (middle for one view and bottom rotating the cylinder by 180°).

4 Documentation of sector-map code

Most of the `root`-based code described here is located in a github repository [30]. We will in the following refer to

```
sphenix_cosmics
```

as the main directory.

4.1 Input data and map generation

The input data to generate the sector maps stem from the following sources:

1. UIUC EMCal block database - a google sheet (Sec. 2.4)
2. Cosmic runs at BNL / SDDC (Sec. 2.6)
3. The **skimmed database** is another google sheet [31] that combines and cherry-picks from 1. and 2..

In the skimmed database, the blocks are rolled out in a 1-dimensional array in the order A1, B1, C1, D1, A2, ..., A24, B24, C24, D24 in the order of sector serial number, starting with Sector 1 and ending with Sector 64, 6,144 blocks in total. The columns from the google sheet are then manually fed into a `csv` file located here:

```
sphenix_cosmics/emcal_plots/sPHENIX_EMCal_blocks - dbn_mpv.csv
```

From there, the maps are filled, following the sequence:

1. update `files/physics_runs.csv` if needed (sector → run number mapping)
2. while on SDCC, run `bnl_copy_phys_runs.cpp` if needed (copies any run folders not existing locally)
3. run `todo.cpp` (extracts MPV from histograms for each sector and outputs to `files/dbn_mpv.csv`)
4. open `files/dbn_mpv.csv` with a spreadsheet viewer such as excel, copy all data, and paste into skimmed database using option "Values only"
5. in skimmed database, do **Extensions** → **Apps Script** and click **Run** with function `getMap` selected in the top toolbar (copies remaining fields from our database)
6. download skimmed database as csv and move to `files` directory
7. run `emcal_plots/plot.cpp`

Plots are generated in

```
emcal_plots
```

with macro

```
emcal_plots/plot.cpp
```

The data in the skimmed DB from Sec. 4.1 is stored in a structure called

```
typedef struct Block {
...
} Block;
```

where the "..." correspond to exactly the entries in the skimmed DB, in that order. If it should in the future be desired to add more block or channel properties as additional columns in the skimmed DB, the code has to be changed here accordingly.

The author of the code logs in to BNL / SDDC with a "nomachine connection" and copies new cosmic runs into his laptop github directory, from where the files are uploaded into the github repository. The directory "physics_runs" is assumed to exist. The function

```
get_physics_runs()
```

to copy runs is in

```
includes/mpv_dbn.cpp
```

There is a separate `python` framework available on Google Colab [32] to produce plots from the skimmed database.

4.2 Switching between channels and blocks

The natural granularity of cosmic MPV is the *MPV per channel* since this is how the data are collected in the first place: one measurement per readout channel (see Fig. 2.7). The MPV_i for ADC channel i is determined as the mean of a Gaussian fit to the ADC distribution, and the uncertainty of the MPV measurement for channel i, $\delta\mathrm{MPV}_i$, is the fit uncertainty of the Gaussian mean parameter.

For certain applications it is more useful to look at block level. To obtain the MPV of a given block, $\mathrm{MPV}_{\mathrm{DBN}}$, the participating channels i are averaged:

$$\mathrm{MPV}_{\mathrm{DBN}} = \frac{1}{n}\sum_{i=1}^{n}\mathrm{MPV}_i, \tag{4.1}$$

where $n = 4$ by for blocks that are not edge blocks of the sector, and $n < 4$ (as small as 1) for blocks on the edge of the calorimeter sectors, skipping the edge channels in the averaging process. An exception in the current cosmic analysis framework are the edge channels of the low-rapidity blocks, which are not skipped.

The block-level uncertainty, $\delta\mathrm{MPV}_{\mathrm{DBN}}$, are calculated as follows from the channel-level uncertainties $\delta\mathrm{MPV}_i$:

$$\delta\mathrm{MPV}_{\mathrm{DBN}} = \frac{1}{n}\sum_{i=1}^{n}\delta\mathrm{MPV}_i, \tag{4.2}$$

with $n \leq 4$ the number of contributing channels. The linear sum overestimates the propagated uncertainty and was chosen to have a conservative estimate of the combined uncertainty. Since the individual channel

measurements are independent of each other, the combined uncertainty is smaller in reality and can be calculated from the squares of the individual uncertainties:

$$\delta\mathrm{MPV}_{\mathrm{DBN}} = \frac{1}{N}\sqrt{\sum_{i=1}^{n}\delta\mathrm{MPV}_i^2}, \tag{4.3}$$

but Eq. 4.3 is currently not used.

Equations 4.1 and 4.2 are also applied to obtain the average MPV and its uncertainty over a set of blocks, as done, e.g., for Tab. 2.1.

In the script

```
sphenix_cosmics/includes/mpv_dbn.cpp
```

there are functions that look up the block number (DBN) from a given channel, or look up the channel numbers of a given DBN:

```
channel_to_block()
block_to_channel()
```

List of Tables

1.1 EMCal block construction sites and suppliers 10
1.2 EMCal block grading at UIUC 11
2.1 MPVs split up by used scintillating fibers 21
3.1 EMCal sector pairing and numbering schemes 35
A.1 UIUC scintillating-fiber batches S1-12 49
A.2 UIUC scintillating-fiber batches S13-64 part 1 50
A.3 UIUC scintillating-fiber batches S13-64 part 2 51
A.4 UIUC tungsten-powder batches for S1-12 54
A.5 UIUC tungsten-powder batches for S13-64 part 1 55
A.6 UIUC tungsten-powder batches for S13-64 part 2 56
A.7 UIUC epoxy batches 57

List of Figures

1.1 sPHENIX EMCal overview 3
1.2 sPHENIX detector and calorimeter system 4
1.3 Photo of EMCal block with dimensions 5
1.4 EMCal sector and 2D-projectivity 6
1.5 EMCal tower, block, sector and barrel 7
1.6 UIUC EMCal block shipments 12
1.7 EMCal sector and readout channels 14
2.1 1D block distributions 15
2.2 UIUC EMCal block database 17
2.3 Convention for labeling of block positions 18
2.4 Problematic DBNs 19
2.5 EMCal DBN map 20
2.6 EMCal cosmic test stand 21
2.7 MPV extraction sequence 22
2.8 1D MPV distributions 23
2.9 Average MPV versus fiber batch 24
2.10 Initial pre-calibration of EMCal channels 25
2.11 Correlations between MPV and density, light transmission, and scintillation 26
2.12 Correlations between scintillation and light transmission 27

2.13 Correlations between ADC channel and fiber tower 27
3.1 EMCal channels ordering scheme 28
3.2 EMCal maps by sector serial number for density and light transmission 30
3.3 EMCal maps by sector serial number for scintillation and MPV 31
3.4 EMCal maps by sector serial number for MPV with modified trigger scheme 32
3.5 Average MPV and density vs. sector serial number 33
3.6 EMCal sector numbering schemes and locations 34
3.7 EMCal maps by physical sector location for density and scintillation 37
3.8 EMCal maps by physical sector location for light transmission 38
3.9 EMCal maps by physical sector location for MPV 39
3.10 EMCal maps by physical sector location for MPV, fancy representations 40
A.1 UIUC scintillating-fiber batches - distribution over sectors 52
A.2 UIUC tungsten-powder batches - distribution over sectors 53
A.3 UIUC epoxy batches - distribution over sectors 58
B.1 UIUC person power for fiber-set assembly and checking 60
B.2 UIUC person power for mold and tungsten-powder loading, and block potting 61
B.3 UIUC person power for block machining and testing 62

Bibliography

[1] sPHENIX Collaboration, *sPHENIX Technical Design Report* (TDR PD2/3 release May 2019).

[2] sPHENIX Collaboration, *sPHENIX Technical Design Report* (TDR CD2 release February 2019).

[3] C. A. Aidala *et al.*, *Design and Beam Test Results for the sPHENIX Electromagnetic and Hadronic Calorimeter Prototypes*, IEEE Trans. Nucl. Sci. **65**, no.12, 2901-2919 (2018) [arXiv:1704.01461 [physics.ins-det]].

[4] C. A. Aidala *et al.*, *Design and Beam Test Results for the 2-D Projective sPHENIX Electromagnetic Calorimeter Prototype*, IEEE Trans. Nucl. Sci. **68**, no.2, 173-181 (2021), [arXiv:2003.13685 [physics.ins-det]].

[5] sPHENIX Collaboration, *sPHENIX Beam Use Proposal 2022* (BUP 2022)

[6] S. Stoll, *sPHENIX EMCAL - Technical Overview and Applications*, sPHENIX summer school, May 26, 2022.

[7] E. Garutti, *Calorimeters - energy measurement*, lecture 2012, University of Hamburg / DESY.

[8] T. Rinn, *sPHENIX EMCal design, construction and test beam results*, poster presented at the Qaurk Matter conference 2019, Wuhan, China.

[9] X. Wang, *sPHENIX EMCal Design, Construction and Test Beam Results*, poster presented at the RHIC & AGS Annual Users' Meeting 2020.

[10] W. Ma, *sPHENIX EMCal Module Prototyping and Production Plan in China*, poster presented at the 10th International Conference on Hard and Electromagnetic Probes of High Energy Nuclear Collisions (Hard Probes 2020), online.

[11] sPHENIX Collaboration, *block and screen design drawings*, March 2017.

[12] sPHENIX UIUC group, *UIUC EMCal Quality Assurance Plan (QAP)*, July 2020 v2.1.

[13] sPHENIX UIUC group, *EMCal block Standard Operating Procedures (SOPs)*, 2019-2021.

[14] W. Ma, *EMCAL block production: status at Fudan, PKU and CIAE*, talk given at the 10th sPHENIX collaboration meeting, January 2021 (online).

[15] sPHENIX UIUC group, *EMCal block testing manuals*, 2021.

[16] sPHENIX UIUC group, EMCal block testing codes on github, https://github.com/sPHENIX-Collaboration/EMCalProduction.

[17] M. Housenga, *sPHENIX EMCal Block Quality and Data Management*, UIUC undergrad research project spring 2021.

[18] M. Mazeikis, *Block Construction and Testing for the sPHENIX Electromagnetic Calorimeter*, poster presented at the Conference Experience for Undergraduates as part of the virtual American Physical Society Division of Nuclear Physics meeting, 2020, and at the RHIC & AGS Annual Users' Meeting 2020.

[19] M. Housenga, *Quality control of sPHENIX EMCal blocks*, poster presented at the Conference Experience for Undergraduates as part of the virtual American Physical Society Division of Nuclear Physics meeting, 2020, and at the RHIC & AGS Annual Users' Meeting 2020.

[20] UIUC Physics, *High-precision construction of sPHENIX detector components wraps up at NPL*, photo story fall 2021.

[21] C. Riedl, E. Thorsland, A. Sickles, *sPHENIX EMCal absorber block construction*, talk given at the 12th sPHENIX collaboration meeting, January 2022 (online).

[22] sPHENIX UIUC group, *UIUC EMCal block database*, google sheet, 2017-2022.

[23] sPHENIX Fudan University, CIAE, and PKU groups, *Documentation of Fudan and CIAE / PKU EMCal blocks*, excel sheets imported into google sheets, 2020-2022.

[24] sPHENIX EMCal BNL group, *Travelers (block locations) for EMCal sectors 1-32*, excel sheets imported into google sheets, June 14, 2021.

[25] sPHENIX EMCal BNL group, *Travelers (block locations) for EMCal sectors 33-64*, excel sheets imported into google sheets, April 15, 2022.

[26] T. Rinn's cosmic-data webpage, https://sphenix-intra.sdcc.bnl.gov/WWW/user/trinn/cosmic_analysis, 2021-2022. Use proxy in your web browser, `ssh` tunnel to access this webpage - `ssh yourlogin@cssh.rhic.bnl.gov -L 3128:batch3.phy.bnl.gov:3128` - and log in with your SDDC account. Documentation: T. Rinn, talk at EMCal meeting September 3, 2021.

[27] sPHENIX EMCal group, sector raw cosmic data on SDCC, `/gpfs/mnt/gpfs02/sphenix/user/trinn/sPHENIX_emcal_cosmics_sector0/macros/` Output histograms: `/sphenix/user/trinn/sPHENIX_emcal_cosmics_sector0/macros/qa_output_runnumber` The data can be copied away from SDDC to your local system using `sftp -rp` (`scp` does not work).

[28] T. Rinn, sPHENIX EMCal sector installation map, talk given at the EMCal meeting June 10, 2022.

[29] C. Pontieri, P. Hamblen, Commissioning Task Force Cabling Update, commissioning task force meeting July 18, 2022.

[30] M. Housenga's sPHENIX github repository, https://github.com/masonrh2/sphenix_cosmics, 2022.

[31] sPHENIX UIUC group, *UIUC EMCal skimmed database*, google sheet, 2022.

[32] M. Housenga's google Colaboratory script to process the UIUC skimmed DB, https://colab.research.google.com/drive/1VwoDSbU3UM_vvGoQEpTy-s0Y6QdNWxTo?usp=sharing.

A Raw material used at UIUC

UIUC estimates that the average cost per S13-64 EMCal block is $823. This includes the 10% margin accounted for when ordering the raw material (i.e., spares / failures). The actual failure rate was 13.5% for S1-12 blocks (1,152 deliverable blocks) and 4.1% for S13-64 blocks (3,744 deliverable blocks). The average material costs per block for fibers, tungsten and meshes were determined by starting from the overall S13-64 costs and then dividing by the 3,744 deliverable S13-64 blocks. The material costs for epoxy and mold are based on the average used material per block, since these materials were only ordered "as needed". The labor costs are estimated based on the spring 2019 hourly rates and an average time estimate to complete a task.

Not included in this estimate are the costs to set up factory and infrastructure, which requires, amongst others, a well-equipped machine shop, multiple well-lit work stations, space to store tungsten buckets and fiber boxes, a fork truck to move tungsten buckets, a well-ventilated area to fill tungsten powder, and a fume hood to epoxy-cast the blocks.

The $823 per block break down as follows:

- Labor: $122, thereof:
  - Fiber-set assembly: $37
  - Block production: $85
- Material: $701, thereof:
  - Fibers: $406
  - Tungsten: $232
  - Meshes: $36
  - Epoxy: $19
  - Mold: $8

In summary, the three main cost drivers are fibers (49%), tungsten powder (28%), and labor (15%), and the remaining 8% stem from the meshes, epoxy, and mold.

Note that blocks of different designs 123...24 vary in length and volume and therefore in the amount of required material. Here, average required amounts of material are quoted. In the main phase of the project at UIUC, molding forms were re-used between 20 and 80 times.

Details about the material specifications and company contacts can be found in Sec. 1.4.

Scintillating fibers

The scintillating-fiber batches from Saint-Gobain used at UIUC are listed in Tabs. A.1, A.2 and A.3, and their distributions over the different sectors are shown in Fig. A.1. The S1-12 fibers amount to total 800 km and cost $385k. The S13-64 fibers amount to total 1,800 km and cost $840k. About 0.5 km are needed per average block. At UIUC, there are fibers left over to make around 1,300 blocks.

Table A.1: UIUC scintillating-fiber batches from Saint-Gobain for pre-production blocks S1-12. The table includes all blocks (including some prototypes and failing). One pouch ("sleeve") contains 200 fibers of 1.2 m length each. Batches with a "-" in the rightmost column are still available at UIUC.

batch	delivery date	pouches	blocks	last filled
1-A	7/10/2018	81	39	6/26/2019
1-B	7/10/2018	85	40	2/4/2019
2-A	7/17/2018	81	44	6/20/2019
2-B	7/17/2018	86	48	11/21/2019
3-A	7/23/2018	84	49	9/10/2020
3-B	7/23/2018	83	46	6/6/2019
4-A	7/31/2018	83	48	2/21/2019
4-B	7/31/2018	83	48	5/22/2019
5-A	8/7/2018	83	48	9/11/2020
5-B	8/7/2018	84	45	11/20/2020
6-A	8/14/2018	83	46	9/10/2020
6-B	8/14/2018	84	46	4/8/2019
7-A	8/21/2018	84	46	9/10/2020
7-B	8/21/2018	83	44	9/8/2020
8-A	8/28/2018	82	41	9/16/2020
8-B	8/28/2018	84	49	9/15/2020
9-A	9/5/2018	83	52	9/17/2020
9-B	9/5/2018	83	50	6/26/2019
10-A	9/11/2018	84	53	6/26/2019
10-B	9/11/2018	83	49	9/11/2020
11-A	9/18/2018	83	52	9/1/2020
11-B	9/18/2018	84	52	9/1/2020
12-A	9/24/2018	84	54	8/21/2020
12-B	9/24/2018	83	54	9/23/2020
13-A	10/2/2018	83	47	8/28/2020
13-B	10/2/2018	84	47	6/25/2019
14-A	10/9/2018	83	46	6/27/2019
14-B	10/9/2018	84	7	8/19/2020
15-A	10/16/2018	81	0	-
15-B	10/16/2018	84	47	9/3/2020
16-A	10/23/2018	80	40	9/18/2020
16-B	10/23/2018	85	23	10/14/2020
17-A	10/30/2018	83	0	-
17-B	10/30/2018	81	0	-
18-A	11/06/2018	87	0	-
18-B	11/06/2018	81	0	-
19-A	11/14/2018	83	0	-
19-B	11/14/2018	84	0	-
20-A	11/21/2018	82	0	-
20-B	11/21/2018	84	0	-

Table A.2: UIUC scintillating-fiber batches from Saint-Gobain for production blocks S13-64 part 1 (continued in Tab. A.3). The table includes all blocks (including failing). One pouch ("sleeve") contains 200 fibers of 1.2 m length each.

batch	delivery date	pouches	blocks	last filled
21-A	4/7/2019	83	45	7/2/2019
21-B	4/7/2019	82	45	7/9/2019
22-A	4/7/2019	81	44	7/11/2019
22-B	4/7/2019	81	44	7/12/2019
23-A	5/3/2019	80	44	7/24/2019
23-B	5/3/2019	83	46	7/19/2019
24-A	5/3/2019	80	43	7/23/2019
24-B	5/3/2019	84	46	7/26/2019
25-A	6/19/2019	90	48	7/30/2019
25-B	6/19/2019	73	39	8/1/2019
26-A	6/19/2019	83	52	10/27/2021
26-B	6/19/2019	83	42	9/5/2019
27-A	7/17/2019	80	44	9/6/2019
27-B	7/17/2019	83	44	11/3/2021
28-A	7/17/2019	83	38	9/17/2021
28-B	7/17/2019	82	41	12/11/2020
29-A	8/20/2019	80	46	11/2/2020
29-B	8/20/2019	86	52	7/22/2021
30-A	8/20/2019	90	51	7/8/2021
30-B	8/20/2019	79	47	1/5/2021
31-A	9/18/2019	71	41	1/20/2021
31-B	9/18/2019	73	40	1/22/2021
32-A	9/18/2019	65	43	9/23/2020
32-B	9/18/2019	58	34	6/18/2021
32-C	9/18/2019	60	43	2/15/2021
33-A	10/18/2019	66	32	8/13/2020
33-B	10/18/2019	66	41	8/5/2020
34-A	10/18/2019	65	45	3/31/2021
34-B	10/18/2019	61	40	9/2/2020
34-C	10/18/2019	67	38	7/23/2020
35-A	11/19/2019	56	33	3/10/2021
35-B	11/19/2019	63	39	7/20/2020
36-A	11/19/2019	68	44	7/15/2020
36-B	11/19/2019	62	38	7/10/2020
36-C	11/19/2019	69	48	7/6/2020
37-A	1/2/2020	67	40	6/11/2020
37-B	1/2/2020	68	42	6/18/2020
38-A	1/2/2020	69	34	11/24/2021
38-B	1/2/2020	59	35	6/23/2020
38-C	1/2/2020	64	39	6/29/2020
39-A	1/16/2020	63	31	4/26/2021
39-B	1/16/2020	64	33	4/26/2021
40-A	1/16/2020	64	38	7/6/2020
40-B	1/16/2020	66	41	3/23/2021
40-C	1/16/2020	69	38	12/10/2020
41-A	2/20/2020	67	42	3/12/2021
41-B	2/20/2020	64	41	8/26/2021
42-A	2/20/2020	64	29	5/25/2021
42-B	2/20/2020	64	40	3/4/2021
42-C	2/20/2020	67	40	2/19/2021
43-A	3/15/2020	63	37	12/6/2021
43-B	3/15/2020	70	43	2/24/2021
44-A	3/15/2020	63	38	8/27/2021
44-B	3/15/2020	62	39	2/3/2021
44-C	3/15/2020	72	43	10/5/2020

Table A.3: UIUC scintillating-fiber batches from Saint-Gobain for production blocks S13-64 part 2 (part 1 is in Tab. A.2). The table includes all blocks (including failing). One pouch ("sleeve") contains 200 fibers of 1.2 m length each. Batches with a "-" in the rightmost column are still available at UIUC.

batch	delivery date	pouches	blocks	last filled
45-A	5/15/2020	71	39	11/13/2020
45-B	5/15/2020	75	44	12/11/2020
46-A	5/15/2020	62	31	9/2/2021
46-B	5/15/2020	67	36	9/7/2021
46-C	5/15/2020	69	32	11/17/2021
47-A	5/20/2020	65	37	12/13/2020
47-B	5/20/2020	68	42	12/23/2020
48-A	5/20/2020	59	36	9/14/2021
48-B	5/20/2020	71	41	10/20/2021
48-C	5/20/2020	48	29	1/15/2021
49-A	6/18/2020	68	41	6/23/2021
49-B	6/18/2020	70	41	9/16/2021
50-A	6/18/2020	61	37	2/5/2021
50-B	6/18/2020	63	31	6/22/2021
50-C	6/18/2020	65	43	2/15/2021
51-A	7/25/2020	70	44	9/27/2021
51-B	7/25/2020	66	37	6/7/2021
52-A	7/25/2020	64	53	3/5/2021
52-B	7/25/2020	64	28	6/3/2021
52-C	7/25/2020	63	38	5/26/2021
53-A	8/18/2020	65	24	1/31/2022
53-B	8/18/2020	64	42	10/27/2021
54-A	8/18/2020	66	30	1/31/2022
54-B	8/18/2020	68	42	5/3/2021
54-C	8/18/2020	64	41	4/28/2021
55-A	9/17/2020	63	35	1/31/2022
55-B	9/17/2020	64	27	1/31/2022
56-A	9/17/2020	63	25	12/20/2021
56-B	9/17/2020	67	43	5/11/2021
56-C	9/17/2020	66	29	12/10/2021
57-A	10/23/2020	72	38	1/24/2022
57-B	10/23/2020	65	41	12/3/2021
58-A	10/23/2020	61	37	6/4/2021
58-B	10/23/2020	65	37	4/26/2021
58-C	10/23/2020	66	32	12/10/2021
59-A	11/24/2020	62	42	12/17/2021
59-B	11/24/2020	65	40	4/15/2021
60-A	11/24/2020	66	39	12/23/2021
60-B	11/24/2020	68	29	1/31/2022
60-C	11/24/2020	64	39	11/17/2021
61-A	1/4/2021	69	0	-
61-B	1/4/2021	65	0	-
62-A	1/4/2021	59	0	-
62-B	1/4/2021	65	0	-
62-C	1/4/2021	68	0	-
63-A	1/26/2021	64	to Fudan	
63-B	1/26/2021	64	to Fudan	
64-A	1/26/2021	70	to Fudan	
64-B	1/26/2021	67	to Fudan	
64-C	1/26/2021	67	to Fudan	
65-A	2/23/2021	61	0	-
65-B	2/23/2021	45	0	-
66-A	2/23/2021	67	38	7/14/2021
66-B	2/23/2021	67	0	-
66-C	2/23/2021	64	0	-
67-A	6/7/2021	from UCLA	26	1/27/2022
67-B	6/7/2021	from UCLA	0	-
68-A	6/7/2021	from UCLA	35	9/2/2021
68-B	6/7/2021	from UCLA	37	7/14/2021
68-C	6/7/2021	from UCLA	42	12/8/2021

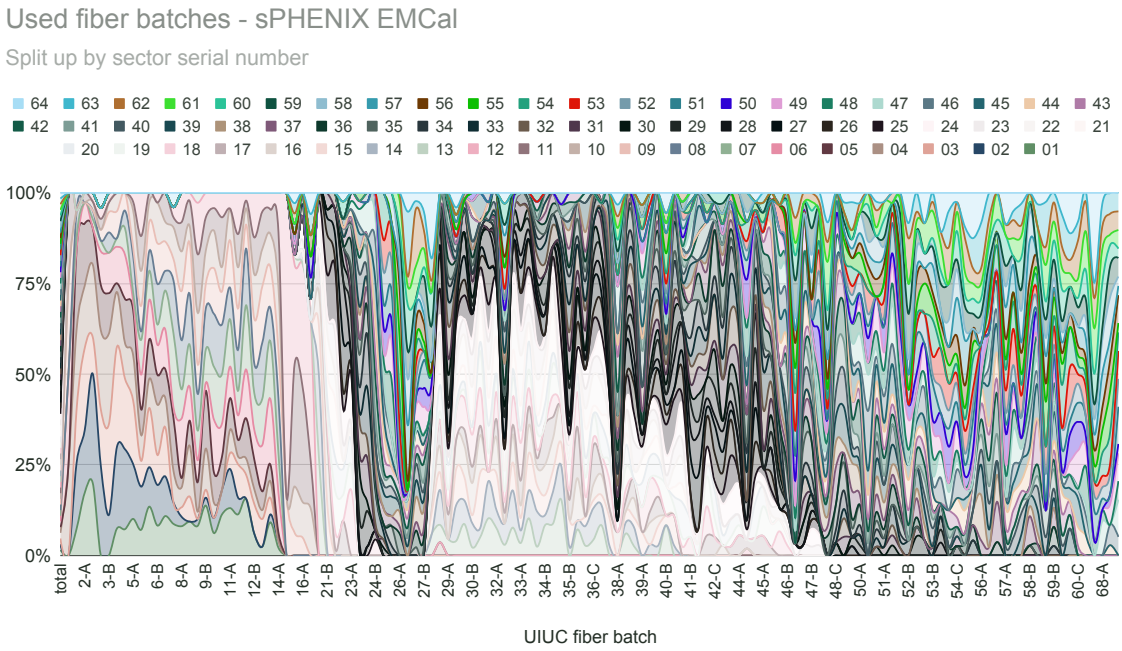

Figure A.1: UIUC scintillating-fiber batches from Saint-Gobain and their distribution over sectors as ordered by sector serial numbers.

Brass meshes

The brass meshes ("screens") that hold the fibers in place were custom-ordered from Tech Etch and were delivered to UIUC about one set per week between November 2018 and April 2019. Here, "one set" refers to one block type (123...24), and there are six distinctive screens of different design per block type. A fraction of the high-rapidity screens 19...24 was later sent to Fudan University. The screens for BL 123 were ordered in triple quantity. The total cost was around \$222k, where one 123 screen was \$4.04 and one 4...24 screen \$5.66, which is relatively low due to the high number of identical screens ordered. The small number of screens ordered for the prototyping was about a factor of ten more expensive per screen. This is due to the manufacturing process, which involves loading the design for each screen into a machine and then photo etching the holes and other patterns into the brass plates. Due to the higher failure rate in S1-12 blocks, a smaller batch was ordered in spring 2021 with per-mesh cost between \$24 and \$41. At UIUC, there are screens left over to make around 500 blocks (mostly for designs 123...18, between 20 and 75 per design).

Tungsten powder

The tungsten-powder batches from H.C. Starck used at UIUC are listed in Tabs. A.4, A.5, and A.6 and their distributions over the different sectors are shown in Fig. A.2. The tungsten powder was ordered in three portions: for Sectors 1-3 (1,200 kg for \$73k at \$60.95/kg), Sectors 4-12 plus half of S13-64 (11,400 kg for \$660.1k at \$57.95/kg), and the second half of S13-63 (8,200 kg for \$489.4 at \$59.68/kg). In a conservative estimate, around 400 kg are needed for a full sector with blocks 123...24, and 300 kg for a "descoped" sector with blocks 123...18. During the main phase of block production at UIUC, these

numbers were significantly lower due to smaller top portions of the unmolded blocks, which are anyway machined away and was as low as 281 kg per (descoped) S13-64 sector. In average, this amounted to 3.91 kg of tungsten powder per 123...18 block. At UIUC, there is tungsten powder left over to make around 200 blocks.

H.C. Starck was very generous and took back the original batch for part 2 of S13-64 tungsten powder. UIUC had found that this batch contained too small tungsten particles, which made the potting procedure extremely difficult to impossible since the epoxy could not sufficiently be pulled out from the bottom of the mold, being hindered by the too fine powder. HCS re-sieved the entire batch to filter out too small tungsten particles. Without additional costs, they also replaced the missing (filtered out) mass with tungsten powder of desired or acceptable particle sizes and returned the replaced batch from Canada to UIUC.

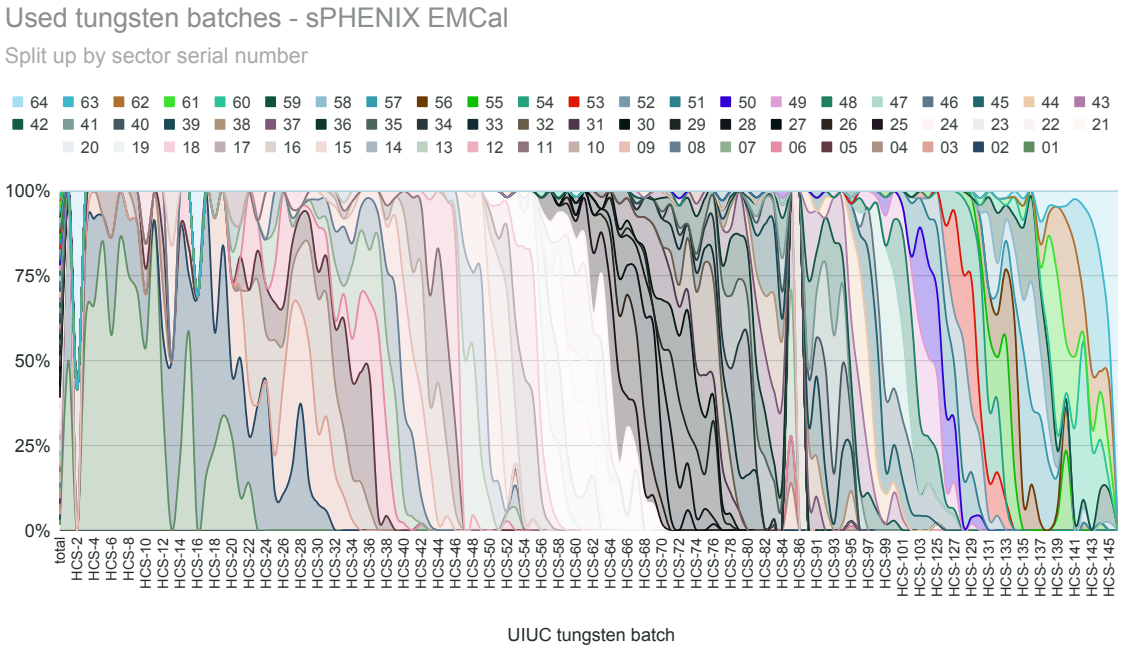

Figure A.2: UIUC tungsten-powder batches from H.C. Starck and their distribution over sectors as ordered by sector serial numbers.

Table A.4: UIUC tungsten-powder for S1-12 from H.C. Starck. A sample was saved from every drum or bucket. TD = tap density in units of g/cm^3. The table includes all blocks (including some prototypes and failing).

batch	HCS batch	delivery	mass [kg]	TD (HCS)	TD (UIUC meas.)	blocks
HCS-0	W5463	3/1/2018	5	10.4	10.5	1
HCS-1	W5463	6/1/2018	32	10.4	10.5	9
HCS-2	W5463	6/1/2018	32	10.4	10.5	7
HCS-3	W5897	10/1/2018	50	10.4	10.5	14
HCS-4	W5897	10/1/2018	50	10.4	10.5	13
HCS-5	W5897	10/1/2018	50	10.4	10.5	17
HCS-6	W5897	10/1/2018	50	10.4	10.5	12
HCS-7	W5897	10/1/2018	50	10.4	10.5	8
HCS-8	W5897	10/1/2018	50	10.4	10.5	14
HCS-9	W5897	10/1/2018	50	10.4	10.5	12
HCS-10	W5897	10/1/2018	50	10.4	10.5	13
HCS-11	W5897	10/1/2018	50	10.4	10.5	12
HCS-12	W5897	10/1/2018	50	10.4	10.5	16
HCS-13	W5897	10/1/2018	50	10.4	10.5	13
HCS-14	W5897	10/1/2018	50	10.4	10.5	12
HCS-15	W5897	10/1/2018	50	10.4	10.5	13
HCS-16	W5897	10/1/2018	50	10.4	10.5	13
HCS-17	W5897	10/1/2018	50	10.4	10.5	8
HCS-18	W5897	10/1/2018	50	10.4	10.5	13
HCS-19	W5897	10/1/2018	50	10.4	10.5	8
HCS-20	W5897	10/1/2018	50	10.4	10.5	14
HCS-21	W5897	10/1/2018	50	10.4	10.5	13
HCS-22	W5897	10/1/2018	50	10.4	10.5	12
HCS-23	W5897	10/1/2018	50	10.4	10.5	14
HCS-24	W5897	10/1/2018	50	10.4	10.5	12
HCS-25	W5897	10/1/2018	50	10.4	10.5	13
HCS-26	W5897	10/1/2018	50	10.4	10.5	13
HCS-27	W6586	10/29/2019	200	>10	10.5	49
HCS-28	W6586	10/29/2019	200	>10	10.5	49
HCS-29	W6586	10/29/2019	200	>10	10.5	49
HCS-30	W6586	10/29/2019	200	>10	10.6	48
HCS-31	W6586	10/29/2019	200	>10	10.6	49
HCS-32	W6586	10/29/2019	200	>10	10.6	51
HCS-33	W6586	10/29/2019	200	>10	10.6	51
HCS-34	W6586	10/29/2019	200	>10	10.7	46
HCS-35	W6586	10/29/2019	200	>10	10.7	52
HCS-36	W6586	10/29/2019	200	>10	10.6	50
HCS-37	W6586	10/29/2019	200	>10	10.5	48
HCS-38	W6586	10/29/2019	200	>10	10.6	50
HCS-39	W6586	10/29/2019	200	>10	10.6	52
HCS-40	W6586	10/29/2019	200	>10	10.6	47
HCS-41	W6586	10/29/2019	200	>10	10.7	51
HCS-42	W6586	10/29/2019	200	>10	10.7	50
HCS-43	W6586	10/29/2019	200	>10	10.6	53
HCS-44	W6586	10/29/2019	200	>10	10.7	55
HCS-45	W6586	10/29/2019	200	>10	10.7	49
HCS-46	W6586	10/29/2019	200	>10	10.7	52
HCS-47	W6586	10/29/2019	200	>10	10.7	54
HCS-48	W6586	10/29/2019	200	>10	10.7	52
HCS-49	W6586	10/29/2019	200	>10	10.7	53
HCS-50	W6586	10/29/2019	200	>10	10.7	53
HCS-51	W6586	10/29/2019	200	>10	10.7	52
HCS-52	W6586	10/29/2019	200	>10	10.6	58

Table A.5: UIUC tungsten-powder for S13-64 part 1 from H.C. Starck. A sample was saved from every drum or bucket. TD = tap density in units of g/cm^3. The table includes all blocks (including failing).

batch	HCS batch	delivery	mass [kg]	TD (HCS)	TD (UIUC meas.)	blocks
HCS-53	W6617	11/30/2019	200	>10	10.4	52
HCS-54	W6617	11/30/2019	200	>10	10.4	49
HCS-55	W6617	11/30/2019	200	>10	10.5	50
HCS-56	W6617	11/30/2019	200	>10	10.5	53
HCS-57	W6617	11/30/2019	200	>10	10.7	56
HCS-58	W6617	11/30/2019	200	>10	10.5	53
HCS-59	W6617	11/30/2019	200	>10	10.5	53
HCS-60	W6617	11/30/2019	200	>10	10.6	59
HCS-61	W6617	11/30/2019	200	>10	10.6	51
HCS-62	W6617	11/30/2019	200	>10	10.6	47
HCS-63	W6617	11/30/2019	200	>10	10.5	58
HCS-64	W6617	11/30/2019	200	>10	10.5	51
HCS-65	W6617	11/30/2019	200	>10	10.5	56
HCS-66	W6617	11/30/2019	200	>10	10.5	49
HCS-67	W6617	11/30/2019	200	>10	10.5	60
HCS-68	W6617	11/30/2019	200	>10	10.5	53
HCS-69	W6617	11/30/2019	200	>10	10.5	50
HCS-70	W6617	11/30/2019	200	>10	10.5	56
HCS-71	W6617	11/30/2019	200	>10	10.5	56
HCS-72	W6617	11/30/2019	200	>10	10.4	50
HCS-73	W6617	11/30/2019	200	>10	10.5	53
HCS-74	W6617	11/30/2019	200	>10	10.5	57
HCS-75	W6617	11/30/2019	200	>10	10.5	50
HCS-76	W6617	11/30/2019	200	>10	10.5	56
HCS-77	W6617	11/30/2019	200	>10	10.5	40
HCS-78	W6617	11/30/2019	200	>10	10.5	66
HCS-79	W6617	11/30/2019	200	>10	10.5	54
HCS-80	W6617	11/30/2019	200	>10	10.6	55
HCS-81	W6617	11/30/2019	200	>10	10.6	55
HCS-82	W6617	11/30/2019	200	>10	10.6	53
HCS-83	W6617	11/30/2019	200	>10	10.5	54

Table A.6: UIUC tungsten-powder for S13-64 part 2 from H.C. Starck. A sample was saved from every drum or bucket. TD = tap density in units of g/cm^3. The table includes all blocks (including failing). Batches HCS-85 to HCS-89 and HCS-105 to HCS-124 were returned to HCS for re-sieving and are excluded from this table. The buckets with zero blocks are still available at UIUC.

batch	HCS batch	delivery	mass [kg]	TD (HCS)	TD (UIUC meas.)	blocks
HCS-84	W6832	6/5/2020	200	>10	10.8	51
HCS-90	W6832	6/5/2020	200	>10	10.8	51
HCS-91	W6832	6/5/2020	200	>10	10.7	52
HCS-92	W6832	6/5/2020	200	>10	10.8	53
HCS-93	W6832	6/5/2020	200	>10	10.8	54
HCS-94	W6832	6/5/2020	200	>10	10.7	52
HCS-95	W6832	6/5/2020	200	>10	10.7	56
HCS-96	W6832	6/5/2020	200	>10	10.8	50
HCS-97	W6832	6/5/2020	200	>10	10.7	56
HCS-98	W6832	6/5/2020	200	>10	10.9	53
HCS-99	W6832	6/5/2020	200	>10	10.8	57
HCS-100	W6832	6/5/2020	200	>10	10.8	36
HCS-101	W6832	6/5/2020	200	>10	10.8	63
HCS-102	W6832	6/5/2020	200	>10	10.7	57
HCS-103	W6832	6/5/2020	200	>10	10.8	49
HCS-104	W6832	6/5/2020	200	>10	10.8	52
HCS-125	W6923	9/17/2020	200	11	10.6	54
HCS-126	W6923	9/17/2020	200	11	10.7	53
HCS-127	W6923	9/17/2020	200	11	10.7	52
HCS-128	W6923	9/17/2020	200	11	10.8	55
HCS-129	W6923	9/17/2020	200	11	10.7	53
HCS-130	W6923	9/17/2020	200	11	10.7	49
HCS-131	W6923	9/17/2020	200	11	10.7	56
HCS-132	W6923	9/17/2020	200	11	10.8	49
HCS-133	W6923	9/17/2020	200	11	10.7	52
HCS-134	W6923	9/17/2020	200	11	10.7	55
HCS-135	W6923	9/17/2020	200	11	10.6	50
HCS-136	W6923	9/17/2020	200	11	10.6	57
HCS-137	W6923	9/17/2020	200	11	10.7	49
HCS-138	W6923	9/17/2020	200	11	10.6	51
HCS-139	W6923	9/17/2020	200	11	10.6	51
HCS-140	W6923	9/17/2020	200	11	10.7	53
HCS-141	W6923	9/17/2020	200	11	10.7	52
HCS-142	W6923	9/17/2020	200	11	10.7	50
HCS-143	W6923	9/17/2020	200	11	10.9	55
HCS-144	W6923	9/17/2020	200	11	10.9	50
HCS-145	W6923	9/17/2020	200	11	10.9	49
HCS-146	W6923	9/17/2020	200	11	10.8	19
HCS-147	W6923	9/17/2020	200	11	10.8	0
HCS-148	W6923	9/17/2020	200	11	10.9	0
HCS-149	W6923	9/17/2020	200	11	10.8	0

Epoxy

The epoxy batches from Epoxy Technology used at UIUC are listed in Tab. A.7 and their distributions over the different sectors are shown in Fig. A.3. The cost per lbs was between $46.55 and $55, with a tendency to bulk prices for larger quantities. There was a severe shortage of epoxy in fall of 2021, shortly before the end of the project, and it was not straight forward to receive the final amount needed to complete all blocks. It is advisable to plan well between having a good supply at hand at the lab, and shelf life time. UIUC was able to complete the project on time only due to the excellent customer relations with Epoxy Technology, and a highly motivated person at that company.

Table A.7: UIUC epoxy batches from Epoxy Technology. The table includes all blocks (including some prototypes and failing). The indicated mass is for the resin (part A).

batch	blocks potted	mass [lbs]	date ordered	date received	expiration date	first block potted	last block potted	weeks used
2	31	10		11/2017				84
3	113	40		9/13/2018				44
4	116	40	3/26/2019	4/11/2019	3/27/2020	5/10/2019	10/11/2019	22
5	113	40	8/1/2019	8/26/2019	6/8/2020	9/24/2019	11/22/2019	8
6	273	80	10/16/2019			11/26/2019	5/5/2020	23
7	284	80	2/10/2020	3/19/2020		5/5/2020	7/2/2020	8
8	847	240	3/23/2020	4/20/2020		10/1/2020	1/7/2021	14
9	789	240	8/25/2020	9/22/2020	8/25/2021	11/10/2020	2/26/2021	15
10	868	240	10/13/2020	11/16/2020	10/26/2021	3/1/2021	5/26/2021	12
11	821	240	2/22/2021	4/9/2021		5/26/2021	9/7/2021	15
12	853	240		7/5/2021	6/17/2022	8/10/2021	12/17/2021	18
13	111	30	9/15/2021	10/25/2021	10/15/2022	11/16/2021	12/1/2021	2
14	40	11	11/15/2021	12/3/2021		12/3/2021	12/10/2021	1
15	71	19		12/10/2021		12/10/2021	12/15/2021	1
16	38	15		12/17/2021		12/20/2021	2/5/2022	7

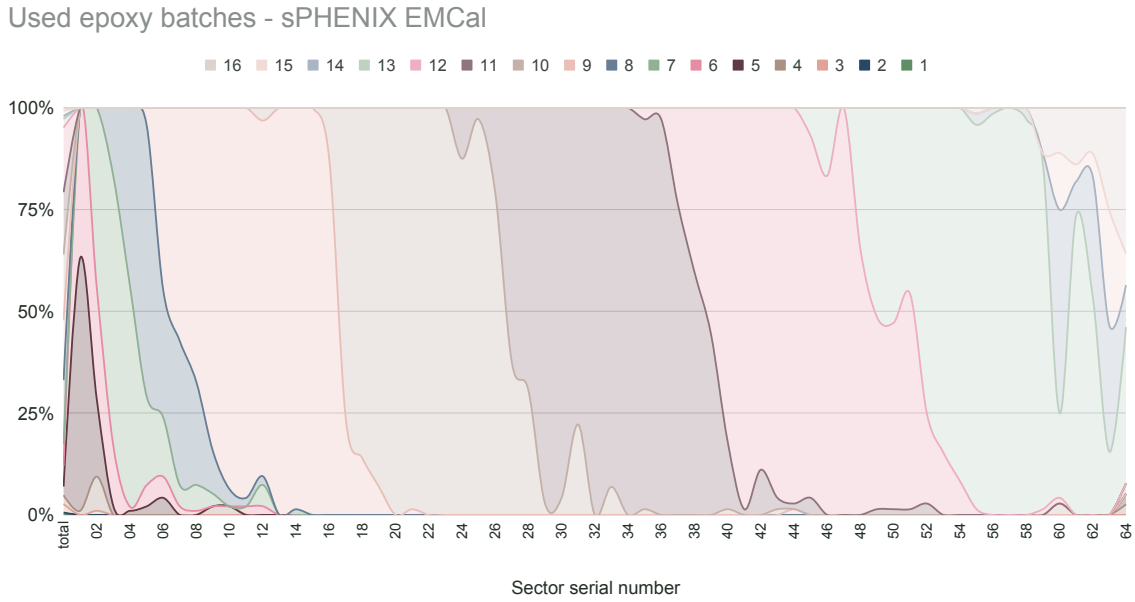

Figure A.3: UIUC epoxy batches and their distribution over sectors as ordered by sector serial numbers.

B Person power at UIUC

The following persons were involved in the EMCal block project at UIUC from 2015 through December 2021, with the superscripts indicating the job position with 1=high-school student (2 total), 2=undergrad student (65 total), 3=master student (3 total), 4= grad student (3 total), 5=postdoc (3 total), 6=technician (10 total), 7=faculty (2 total), with in total 88 persons:

Adam Fowler[2], Adam Wehe (AW)[6], Adin Hrnjic[4], Alec McKay (AM)[2], Alexis Roels[2], Alina Ampeh[2], Amanda Skittone (AS)[2], America Duran[1], Anabel Romero[4], Anmol Raina[2], Anne Sickles[7], Ari Krause[2], Ashlyn Atkison[2], Ben Dibuz[2], Caroline Riedl (CR)[7], Chirag Jain[2], Clayton Curry (CC)[6], Daniel Kaputa[2], Daniel O'Leary[2], Dhriti Gandhi (DG)[2], Dwij Patel[2], Emily Pasetes (EP)[2], Eric Hoshaw[2], Eric Thorsland (ET)[6], Erin Cook (EC)[2], Eyal Friling[2], Fyodor Dugger[2], Gautam Pakala (GP)[2], Gigi Yik[2], Harsha Marupudi[2], Harshit Bagla[2], Henry Markarian[2], Ian Brown[2], Janais Peace[2], Jared Lobo[2], Jeremy Larson (JL)[2], Jerome Tkach (JT/JK)[2], John Blackburn[6], John Farwick[2], Joseph Foy[2], Justin Hubbard[6], Justine Rich[2], Kenan Patel[2], Lucas Reeves (LR)[6], Lucas Trojanowski[3], Maria Sajan[2], Mason Housenga (MH)[2], Matthew Rilloraza (MR)[2], Matthew Steele[2], Michael Higdon[2], Mina Mazeikis (MM)[2], Mona Jawad[1], Mostafa Shehata[2], Nabeeha Ahmed[2], Naman Bhartia[2], Nandini Jain[2], Nic Reeves[6], Nick Talbert[2], Nikita Jain[2], Nur Al-Kodmany[2], Oishee Nandy[2], Parker Hays[2], Peter Sobel[6], Pranav Handa[2], Raihana Hossain[2], Rishi Mishra[2], Ritvik Desai (RD)[2], Saad Altaf (SA)[2,6], Sara Shahid[2], Shanay Gandhi[2], Shanay Patel[3], Shash Sardesai[2], Siddhant Rao[2], Sparsh Srivastava[2], Suhani Jaiswal[2], Tim Rinn (TR)[5], Vedant Agrawal[2], Vera Loggins[5], Vihaan Kalaria[2], Vishwa Mallampooty (VM)[2,6], Vrishin Sutaria (VS)[2], Will Walton (WW)[2], Xiaoning Wang[4], Yatharth Dhoot[2], Yongsun Kim[5], Yuxuan Hu[2], Zander Leja (ZL)[2].

If a person has more than one job position indicated, only the last one is counted. In some of the figures in this section, the name initials are used (indicated in parentheses where applicable).

For each sector, the individual work steps on absorber blocks (as detailed in Sec. 1.4) are split up by person in Figs. B.1 (fiber-set assembly and fiber-set checking), B.2 (loading in mold, tungsten-powder filling, and epoxy casting / potting), and B.3 (machining and testing). Only UIUC blocks that actually made it into sectors are listed, in the figures and in the following itemization, amounting to in total 4,896 blocks.

- The most fiber sets (16.5%) were filled by Erin Cook. 50% of fiber sets were filled by the six leading persons (EC, Saad Altaf, Emily Pasetes, Mason Housenga, Will Walton, and Zander Leja). 49 persons filled the remaining 50% of fiber sets.
- Fiber-set checking: about 50% of the fiber sets were checked by the four leading persons (Saad Altaf, Mason Housenga, Zander Leja, Emily Pasetes) and the other 50% were checked by 75 persons.
- Saad Altaf loaded 75% of all fiber sets in mold. Together with three other persons (Eric Thorsland, Vishwa Mallampooty, and Will Walton), 98% were loaded, and 17 persons loaded the remaining 2%.
- The most tungsten-powder was filled by three persons: Saad Altaf (40%), Eric Thorsland (35%), and Jeremy Larson (18%). The remaining 7% of tungsten powder was filled by seven persons.
- Eric Thorsland epoxy casted ("potted") 73% of all blocks. Saad Altaf casted 23%. Three other persons casted the remaining 4%.
- Pre-production and production blocks were machined by two persons: Adam Wehe, who was involved in the machining of 94% of the blocks, and Lucas Reeves, who was involved in 65%.
- Block testing: 22% of all block tests were carried out by Adam Wehe (dimensional measurements). Other $\sim$ 50% of tests were performed by the four leading persons: Mason Housenga, Mina Mazeikis, Erin Cook, and Zander Leja. The remaining 23% of blocks were tested by 17 further persons.

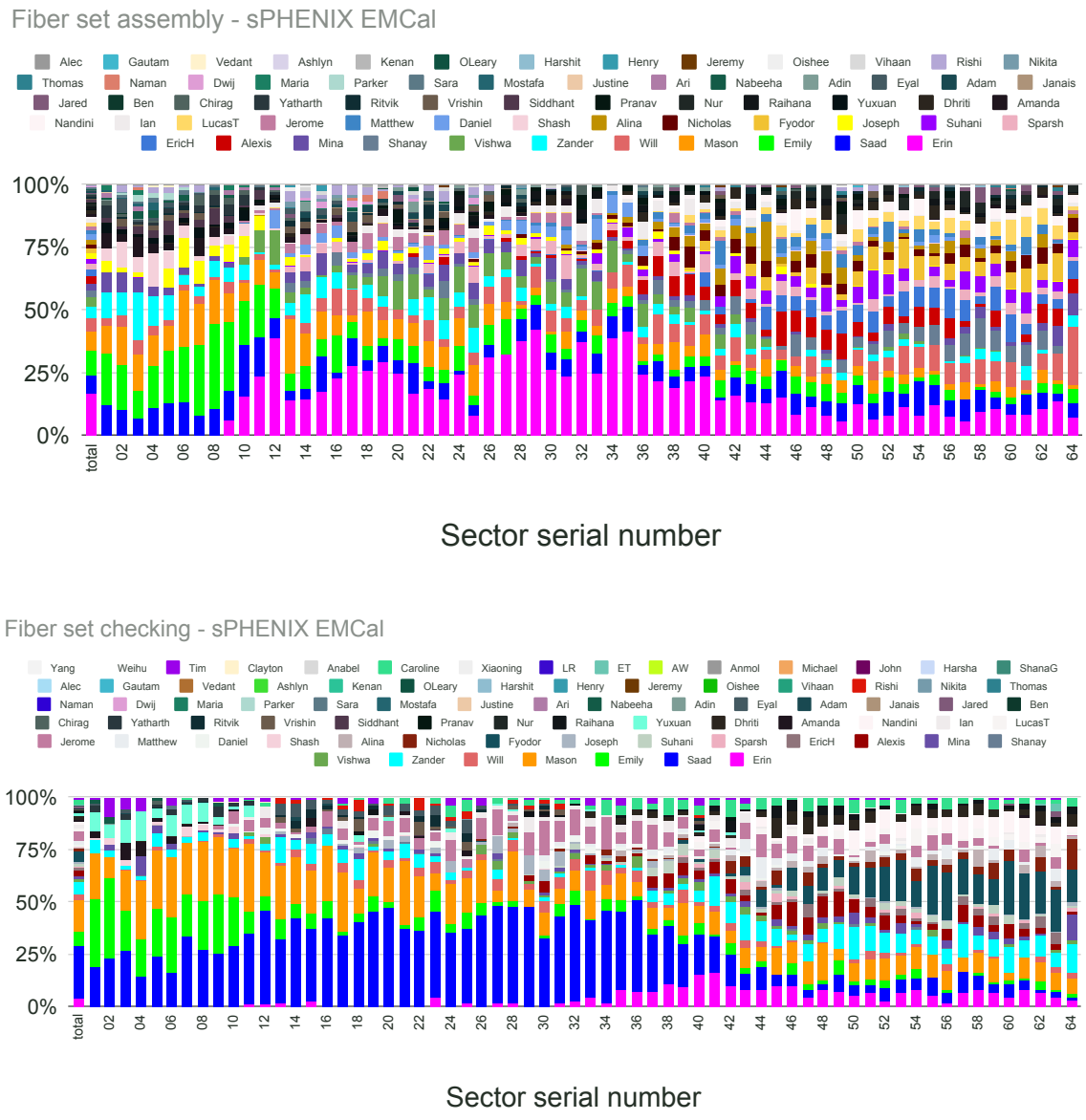

Figure B.1: UIUC person power for fiber-set assembly and checking.

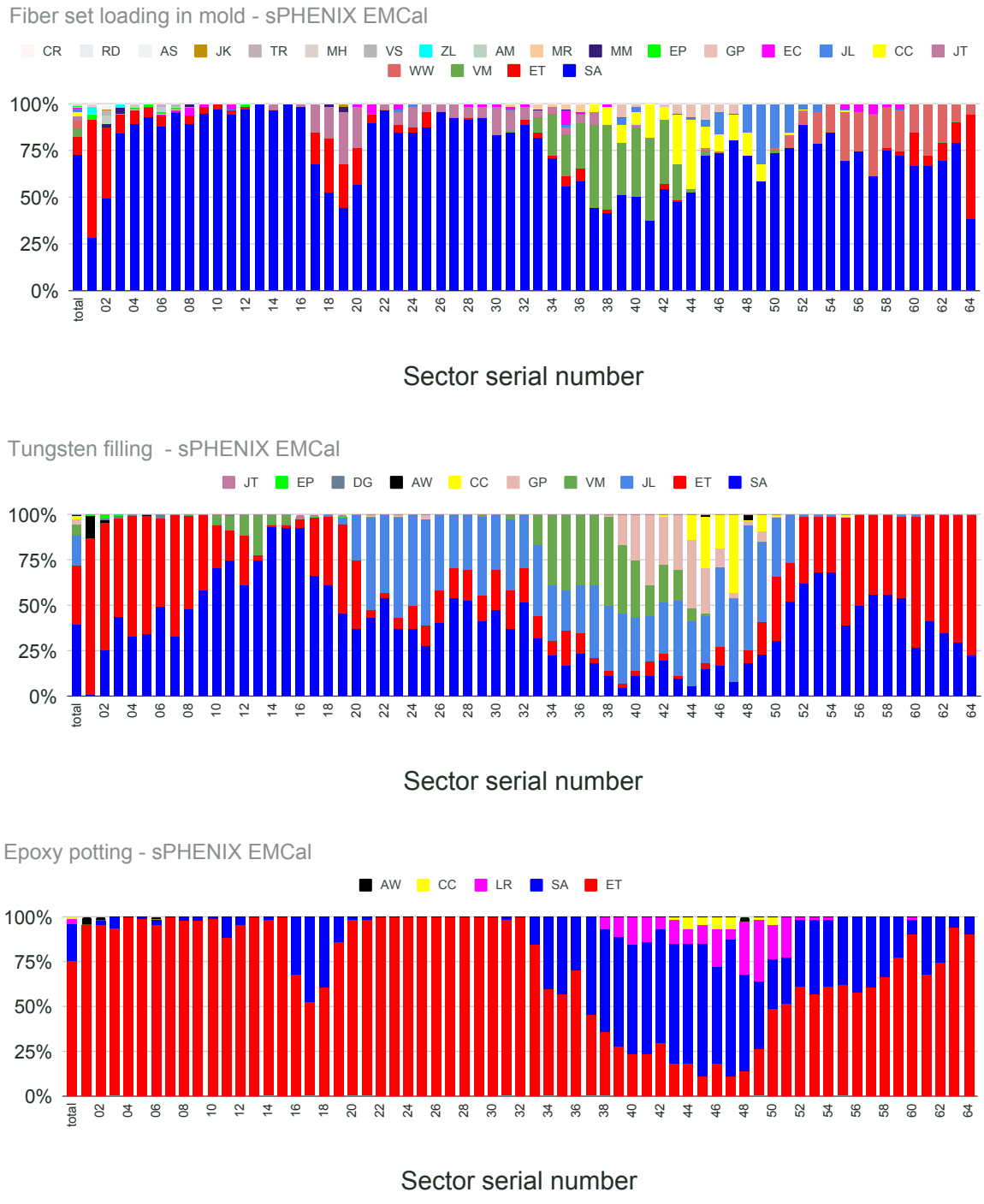

Figure B.2: UIUC person power for mold and tungsten-powder loading, and block potting.

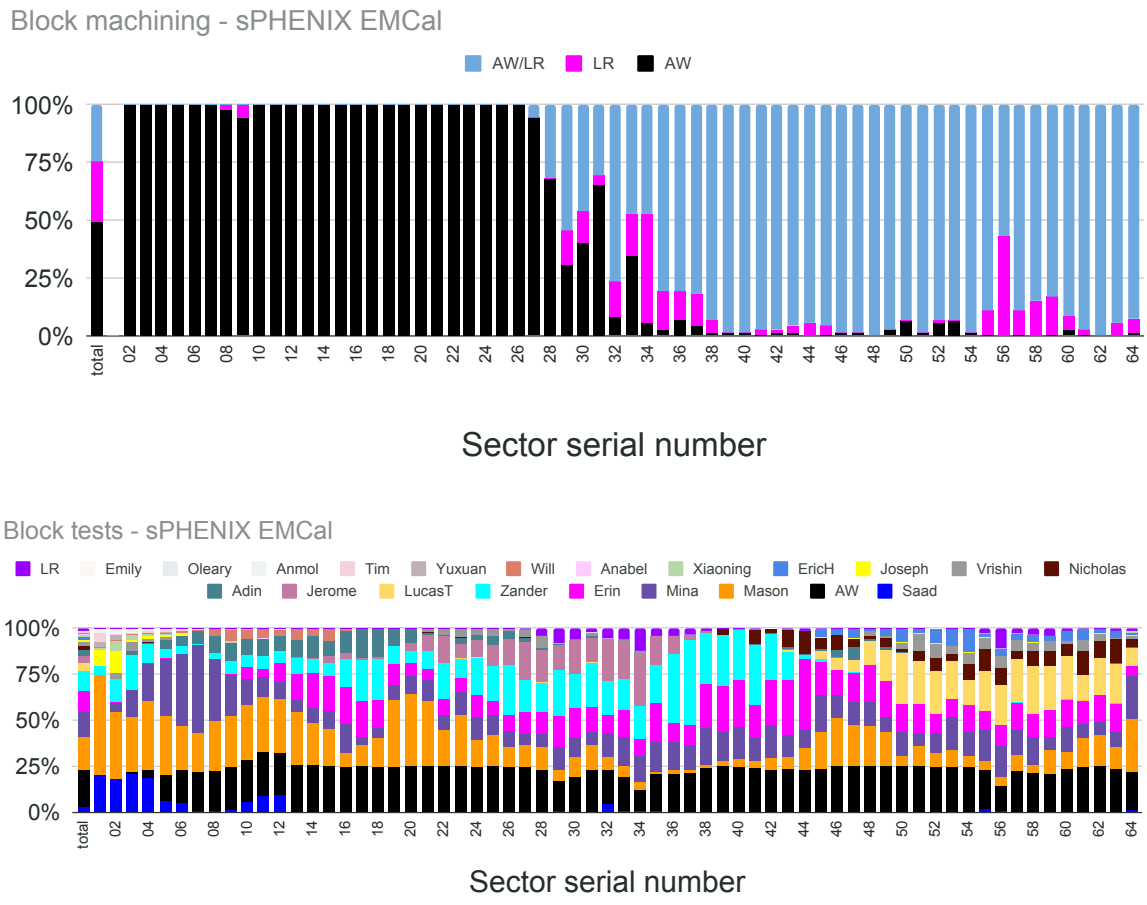

Figure B.3: UIUC person power for block machining and testing.